LA-3434-MS

LOS ALAMOS SCIENTIFIC LABORATORY
of the
University of California
LOS ALAMOS • NEW MEXICO

Semiannual Status Report of the LASL Controlled Thermonuclear Research Program for Period Ending October 31, 1965

UNITED STATES
ATOMIC ENERGY COMMISSION
CONTRACT W-7405-ENG. 36

All LA...MS reports are informal documents, usually prepared for a special purpose. This LA...MS report has been prepared, as the title indicates, to present the status of the LASL program for controlled thermonuclear research. It has not been reviewed or verified for accuracy in the interest of prompt distribution. All LA...MS reports express the views of the authors as of the time they were written and do not necessarily reflect the opinions of the Los Alamos Scientific Laboratory or the final opinion of the authors on the subject.

Printed in USA. Price $3.00. Available from the Clearinghouse for Federal Scientific and Technical Information, National Bureau of Standards, United States Department of Commerce, Springfield, Virginia

LA-3434-MS
UC-20, CONTROLLED
THERMONUCLEAR PROCESSES
TID-4500 (46th Ed.)

LOS ALAMOS SCIENTIFIC LABORATORY
of the
University of California

LOS ALAMOS • NEW MEXICO

Report compiled: November 1965

Report distributed: December 7, 1965

Semiannual Status Report of the LASL Controlled Thermonuclear Research Program for Period Ending October 31, 1965

INTRODUCTION*

(J. L. Tuck)

The last six-month period has been characterized by intense consideration of how to continue our pulsed high density plasma policy in the direction of greater $n\tau$:

(a) By increasing τ, i.e., developing Scylla IV into a closed system - Scyllac, and gun injection into a closed system - Caulked Cusp.

(b) By increasing n, i.e., Columba, Plasma Focus, Explosive Compression of Scylla.

Scylla IV is only now beginning to function to its fully planned extent, i.e., a 0.5-MJ fast θ pinch, with a 3-MJ power crowbar to sustain it. As expected, in mirrorless coils, very little plasma remains at the end of the crowbar phase (17 μsec). However it is still very gratifying that no rotations, filaments, flutes or drifts develop. A large number of experiments are waiting their turn on the Scylla IV machine--including notably studies of the effect of mirrors on the end loss, and side observations of the plasma using quartz confining tubes. It is a strange fact that although other θ-pinch devices of relatively high power but lower E_θ in other laboratories have succeeded in using quartz confining tubes--in Scylla IV at the last attempt, the tube shattered in one shot.

*This section has been reproduced as submitted without any significant editorial changes.

The actual construction of a closed toroidal Scylla will be dependent on three things:

(1) Reasonable results from the plasma confinement at high β in a curved sector shaped Scylla type machine.

(2) Reinforcement from mathematical physical studies of high β plasma stability.

(3) Granting of the funds for (i) the building to house the power supply and apparatus ($1M), (ii) the power supply ($3.5M), and (iii) the Scyllac machine ($1M).

Items (i) and (ii) will be essential even if one of the other pulsed experiments--Caulked Cusp, Columba, dense plasma focus--wins the decisive advantage among the pulsed approaches.

One part of approach (b) already exists in the form of the plasma focus experiment. Another, the Columba experiment, proposes, like (a) to stand on the shoulders of the Scylla IV plasma by applying a z-pinch to it. The Columba proposal discussed in LA-3253-MS Revised is currently in the planning stage and is not mentioned further in this report.

In the plasma focus, we are in urgent need of diagnostic information, notably the plasma density. The delivery of the Mach-Zehnder interferometer which it is hoped will yield this information, is delayed. The plasma focus experiment is a relatively low power one, and it is interesting to explore how it behaves with increase of condenser stored energy. So far the trend of the neutron yield is upward.

A more oblique approach to high n is a collaboration with GMX Division (E. M. Fowler, et al.) to extend the θ-pinch by explosive compression. A voltage doubling θ-pinch bank has been constructed, and the behavior of θ-pinches in special lightly constructed and end fed coils, suitable for explosive compression (LA-3224-MS) is in active investigation. Good plasmas have been obtained; the explosive compression phase should be reached in early 1966.

CAULKED STUFFED CUSP MINIMUM B MACHINE

(L.C. Burkhardt, J.N. DiMarco, H.J. Karr)

A schematic diagram of the caulked stuffed cusp experimental system is shown in Fig. 1. The minimum-B configuration has three field components: (1) a d.c. axial field produced by an 180-turn solenoidal winding around the circumference of the stainless steel vacuum tank, (2) a pulsed field (4×10^{-3} sec half-period) from a four-turn ring coil or "caulking" coil located at the midplane of the assembly, and (3) a pulsed "stuffer" field (8×10^{-3} sec half-period) produced by seven conductors through the tube along the axis of the device.

The resultant field, obtained with the Stretch 7030 computer, is shown in Fig. 2 for one set of field currents. The hatched lines are contours of constant $|B|$ which form nested surfaces around the minimum-B region centered at $r = 27$ cm, $z = 0$. The solid lines are intercepts of the flux surfaces with a plane through the axis of the machine. The field curvature is convex toward the minimum region to afford hydromagnetic stability in this region. Particles leaving the minimum region encounter a mirror ratio of ~ 3 in the axial direction and a ratio of > 6 along field lines encircling the caulking coil. The flux surfaces include a group of "closed" field lines encircling the caulking coil and a second group of "open" field lines outside the closed region. Behavior of plasma in these two regions is of particular interest in this experiment. The method currently under study for filling the minimum B region with plasma is the E x B rotational heating technique in which an electric field is applied between the axial stuffer tube and a Cu coating on the circular caulking coil.

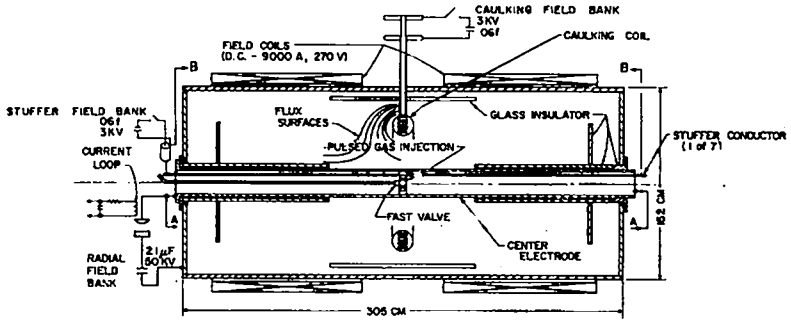

Fig. 1. Caulked stuffed cusp experimental system.

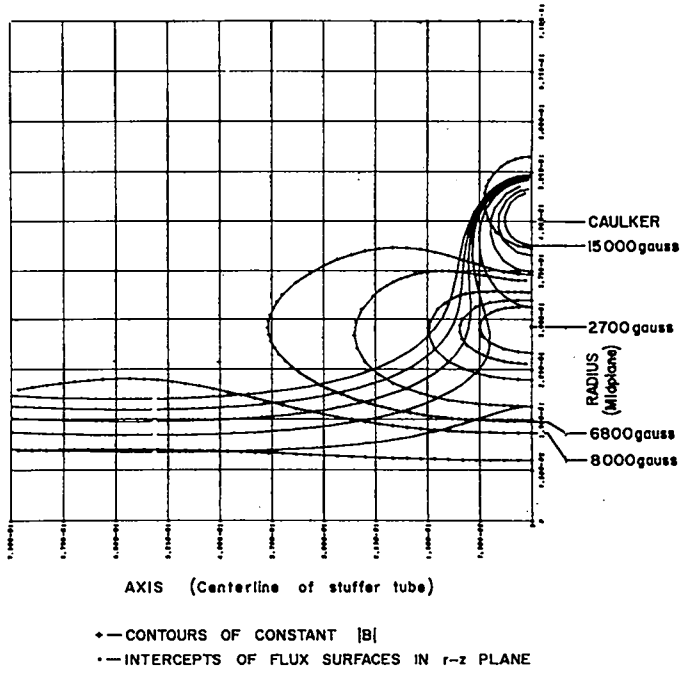

Fig. 2. Quarter section of caulked stuffed cusp magnetic field.

Initial observations of the machine performance were made with time-integrated photographs of the plasma discharge taken through glass ports at the ends of the tank. Typical examples are shown in Fig. 3. It is apparent from Fig. 3c that the discharge streams along the field lines to the support struts of the caulking coil bypassing most of the closed field region. The streaming to the supports was confirmed by means of current distribution measurements made with glass-enclosed Rogowski probes. This effect shorts out the condenser bank intended to supply rotational energy and heating to the plasma.

The support struts to the caulking coil are a major problem. The large magnetic field in this region will restrain much of plasma centered in the system from reaching the struts but some plasma within the closed field region will make contact with them unless they can be shielded. In this experiment, the shielding is made more difficult by the applied radial electric field used in the E x B heating. After gas breakdown, the high conductivity along the field lines causes the latter to become equipotentials; large electric fields thus appear in the region of the supports causing the intense discharges shown in Fig. 3.

The possibility of magnetic shielding of the supports has been mentioned by Lehnert[1] and Kadomstev and Braginsky.[2] Lehnert's method consists in the use of double leads (a magnetic dipole) at each support. The large magnetic fields generated in the region of the double leads act as a screen against particle bombardment. In the plane field approximation for infinitely long leads, the leads can be made approximately force free with a current given by

$$I = 10^7 \, dB_o, \qquad (1)$$

where d = half the distance between centers of the leads and B_o = external field (normal to dipole plane). If this condition is satisfied,

a) Caulked stuffed cusp system viewed through observation port in tank wall with external illumination. Copper-coated ring at the midplane contains the four-turn caulking coil. The ring also serves as an electrode in the plasma discharge. The axial tube serves as the other electrode. The seven stuffer conductors are enclosed in this tube.

b) Plasma luminosity during discharge. Luminous region at axial tube shows bright regions at seven gas injection holes. Second luminous region envelops caulking coil within the "closed" magnetic field region. Transverse photographs show the luminous region extends ~2 in. axially each side of the coil. At the outside, the $\frac{1}{4}$-in. support rods of the coil are luminous over a short portion of their length due to plasma bombardment. (View from other end of tank.)

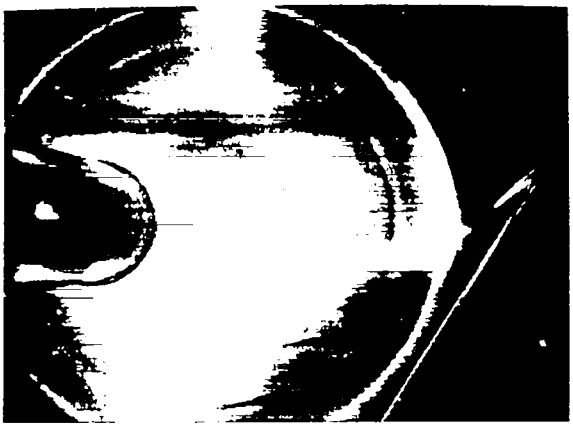

c) Plasma luminosity during discharge at lower gas pressure and lower voltage. Luminous regions are observed to spiral along field lines through closed field region. Impurities are enhanced at support struts. Observe also the shadows cast in the moving plasma by the struts.

Fig. 3. Typical photographs obtained with caulked stuffed cusp system.

the magnetic field lines near the supports close, affording magnetic shielding within a separatrix given by

$$\frac{(x + d)^2 + y^2}{(x - d)^2 + y^2} = e^{x/d}, \qquad (2)$$

where x and y are the coordinates in the plane normal to the dipole with the origin at the dipole axis and the x coordinate is in the plane of the dipole. Field lines outside the separatrix connect with the confinement geometry. The field has a null point on the separatrix at $x = 0$, $y = \pm\sqrt{3}d$.

This shielding method was tested in the caulked stuffed cusp device by insertion of double leads at each of the four support points of the caulker loop with each dipole driven by auxiliary capacitor banks through pulse transformers. For three of the elements, $d \approx 0.008$ m and $B_0 \approx 1$ Wb/m^2, and the force free condition required a current of 8×10^4 A. This affords a shielding field of $\sim 4 \times 10^4$ G at the surface of the leads. The fourth support element, which includes the current feed to the caulker loop, was of larger geometry and required a current of $\sim 2 \times 10^5$ A to satisfy the condition of Eq. (1).

The magnetic shielding was first tested at one of the four supports with apparent success. Three of the supports which were not shielded were subject to the intense discharge from the stuffer electrode along the "closed" field lines to the struts. Results with the magnetically shielded support are shown in Fig. 4. The gas discharge current to the self shielded support measured with a Rogowski loop could not be detected and the visible glow made by the discharge impinging on the strut was removed. This shielding was attainable, however, only for applied voltages, between stuffer electrode and ground, of 3 kV or less. When the shielding was tried with all four double leads activated, it was found to be unsatisfactory. The applied voltage (radial E field), magnetic fields, and dipole currents were varied over a wide range but no adequate shielding

I Caulker = 35 ka
I Solenoid = 800 amps
I Plasma = 6 ka (max)
Voltage on Cap. Bank = 3 kV
Sweep Speeds = 50 μsec/cm

Without Magnetic Shielding Plasma Bombardment of the West Dipole (Upper Left) is Evident

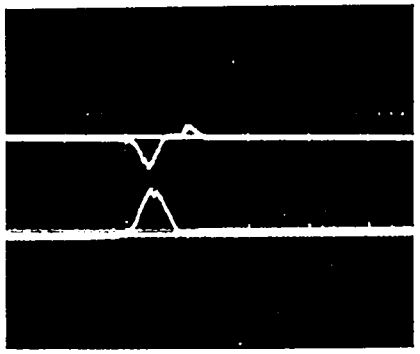

Upper - Current to West Dipole 600 a/cm
Lower - Current to East Dipole 3000 a/cm

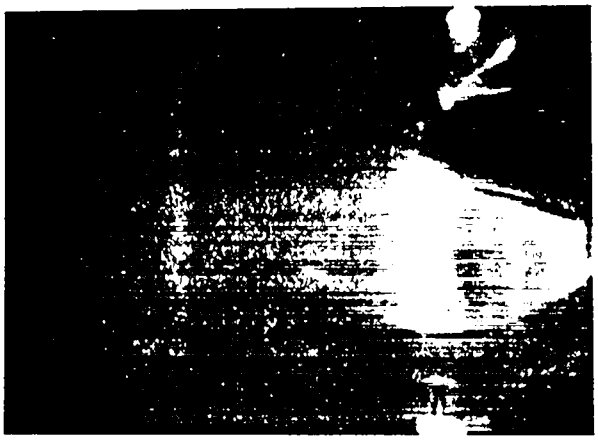

Magnetic Shielding of the West Dipole
I_{dipole} = 18 ka

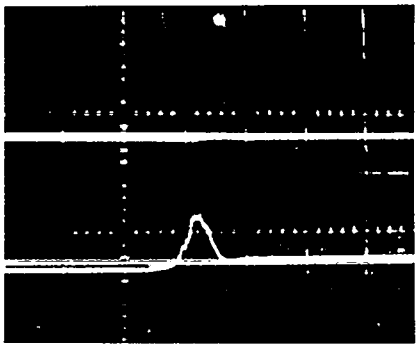

Upper - Current to West Dipole 600 a/cm
Lower - Current to East Dipole 3000 a/cm

Fig. 4. Time integrated photographs showing effect of magnetic shielding on one dipole support.

was obtained. Some effects were observed, such as delay in breakdown indicating hold off of the discharge to the struts for as much as ~ 100 μsec at lower voltages, but the shielding against voltage breakdown does not appear very promising at present.

There are two possible means of electrical breakdown in the region of the magnetic boundary around the double leads that may cause the failure of the shielding. The field lines extending to the region of the stuffer electrode when "loaded" with plasma during the initial ionization process become equipotentials and good conductors. This effect shorts the support to the stuffer electrode, resulting in intense discharges to the unshielded supports. When the support leads are magnetically shielded, the B lines near the separatrix around the leads will be equipotentials at high voltage in this model, and discharge across the shielding field lines to the grounded dipoles will occur if the region contains neutral gas or low-density plasma. This is the type of cross field breakdown observed with the Ixion, Homopolar, and other E x B devices. Another possible discharge region exists in the null region of the separatrix. Any neutral gas in this area may discharge from the "B line equipotentials" to the machine walls or intervening ground points along the magnetic field free null lines. It has not been determined to what extent these effects contribute to the shielding failure. A luminous sheath is observed over the leads extending from the caulker loop surface out into the open field region toward the walls of the tank.

The failure of the magnetic shielding is due to the applied voltages. Results have not indicated that the shielding will be ineffective against plasma without externally applied electric fields. This shielding technique will be tried in the event the experiment is modified to use injected plasma instead of E x B heating.

Attempts have been made to stop the direct discharge along field lines from the stuffer electrode to the caulker supports by using small tubular insulators around the struts as combined insulation and magnetic shielding; so far they have been unsuccessful. The discharge continues over the insulator surface to the caulker surface or outward toward the end of the strut. These insulators have been held to minimum size to decrease the obstruction in the closed field region. Larger insulators, with increased breakdown path length, are being designed for further tests. These will, of course, obstruct the closed field region.

---

[1]B. Lehnert, J. Nucl. Energy, Part C, 1-2, 40 (1959)

[2]B. Kadomstev and S. Braginsky, Proc. of Sec. U.N. Conf. on Peaceful Uses of Atomic Energy, 32, 233 (1958).

ELECTRON-BEAM PLASMA HEATING

(J. McLeod)

The major construction phase of the electron-beam plasma heating experiment is now complete. A high-vacuum electron beam of 1.4 μpervs has been obtained. A fast pulsed gas valve is now in operation and experimentation with neutralization of the electron space charge is now in progress. Such neutralization is required to produce beam currents comparable to those in Nezlin's experiments.[1]

[1]M. V. Nezlin, JETP (Engl. Trans.), 19, 26 (1964).

PLASMA FOCUS EXPERIMENT

(J. W. Mather)

Many of the known properties of the D plasma focus have already been reported,[1] and more recently this work was compared with Filippov's results in the U.S.S.R. at the IAEA Conference at Culham, England.[2] The measurements of the electron temperature and density, volume of region emitting soft x-rays, and the neutron yield and time duration suggest that the plasma focus is a thermal plasma. It is further suggested that the plasma is heated by a fast z-pinch mechanism since the phenomenon occurs at peak current time and follows a sharp decline in the current due to the rapid change in the discharge inductance, i.e., the current pinches to a small diameter. The magnetic energy stored behind the current sheath can by such a mechanism be converted rapidly into sheath motion and plasma energy. One of the most difficult problems of the plasma focus is to account for the long duration[3] of the plasma in comparison with that predicted based on the plasma diameter and local ion speeds. It is believed, but not yet proved, that a finite length z-pinch may offer some confinement due to cold electron flow[4] through the pinched plasma. The neutron yield, although compatible with this thermal plasma assumption, may be due instead to an accelerating mechanism not yet considered. However, this mechanism must show no anisotropy in the angular distribution > 5%, as found experimentally in the U.S.A. and U.S.S.R.

An experiment, using a 50-50 D_2-T_2 gas mixture instead of pure D_2, was performed with the assistance of LASL's W Division. The objectives were to determine (1) if the neutron yield would scale according

to the ratio $\langle\sigma v\rangle_{DT}/\langle\sigma\rangle_{DD}$, and (2) if the lifetime of the plasma focus would increase according to the imperfect knowledge of the finite Larmor radius theory. It was thought that the finite radius effects might already account for some plasma stability in the D-D plasma.

The plasma focus apparatus was redesigned for either a D_2-T_2 gas mixture or for pure D_2. The experiment was carried out without a radiation accident or an electrical failure over a period of 7 days for a total of 300 D-T and 500 D-D discharges. The results are as follows: (1) the neutron yield increased by a factor of 80-100, to $\sim 3 \times 10^{11}$/burst, with D-T compared to D-D at the same operating voltage and initial gas pressure, (2) the lifetime of the plasma, based on the width at half-maximum of the neutron pulse, increased by a factor of ~ 1.5 to ~ 0.22 μsec, and (3) the velocity of the neutrons from a time-of-flight measurement (path length 10.7 m) showed that the neutron energies were compatible with those from the D-T reaction (~ 14 MeV) and of D-D (~ 2.45 MeV).

Probably the most important result of the D-T experiment was the enhanced lifetime of the plasma. A stability calculation[5] of the finite Larmor radius effects based on low-β plasmas showed that the plasma focus parameters did not fit well the stability condition, at least for small values of the azimuthal mode number m. Again, the neutron yield and the yield ratio are easily explained in terms of the assumption of a thermal plasma. An explanation of the neutron yield ratio based on particle acceleration is handicapped by the lack of precise values of the reaction cross sections at low energies (~ 5 keV) for $D(t,n)He^4$ and $T(d,n)He^4$.

Acknowledgments

The valuable assistance is acknowledged of the following: Members of Group W-3, especially R. Stoll; M. Engelke of H-1; and members of Group P-14, especially G. Livermore, A. Schofield, A. Williams, and F. Wittman.

---

[1]Mather, J. W., Phys. of Fluids, 8, 366 (1965).

[2]Plasma Physics and Controlled Nuclear Fusion, IAEA Conference, Culham, England, September 1965 (Proceedings to be published).

[3]Fowler, T.K., Private communication

[4]Furth, H., Private communication

[5]Suydam, B. R., "Finite Larmor Orbit Stabilization," LA-3260-MS (1965).

SCYLLA IV POWER-CROWBARRED MEASUREMENTS

(E.M. Little, W.E. Quinn, F.L. Ribe, G.A. Sawyer)

Introduction

In the last semiannual report (LA-3320-MS, p. 28) separate operation of the 3-MJ secondary bank of Scylla IV was reported. Since then the secondary bank has been successfully used in sequence with the primary bank to provide end-loss and stability measurements of plasma in the low-density regime. A recapitulation of the switching problem and of the experimental results, reported at the 1965 IAEA Conference on Plasma Physics and Controlled Nuclear Fusion Research at Culham, England, is given below.

Operation of the Secondary Capacitor Bank

The secondary bank described previously consists of 21 modules of 700-μF capacitors, each capable of furnishing approximately 1 MA of current to the 1-m compression coil when charged to its maximum energy of 1/7 MJ. The problem of switching these large currents has been discussed by Kemp and Quinn.[1] It was decided to use 21 of the multiple-electrode vacuum spark gaps shown in Fig. 5, each triggered by a stream of plasma fired through the triggering apertures in the plates from the washer-type plasma guns. In a test of the secondary bank alone, switched at 15 kV, the half-period of the current was observed to be 52 μsec, and the measured magnetic field in the compression coil was 121 kG. From the logarithmic decrement of the current wave, a bank resistance $R_s \approx 2.9 \times 10^{-4}$ Ω was derived. The bolted, 4.6-m x 4.6-m parallel-

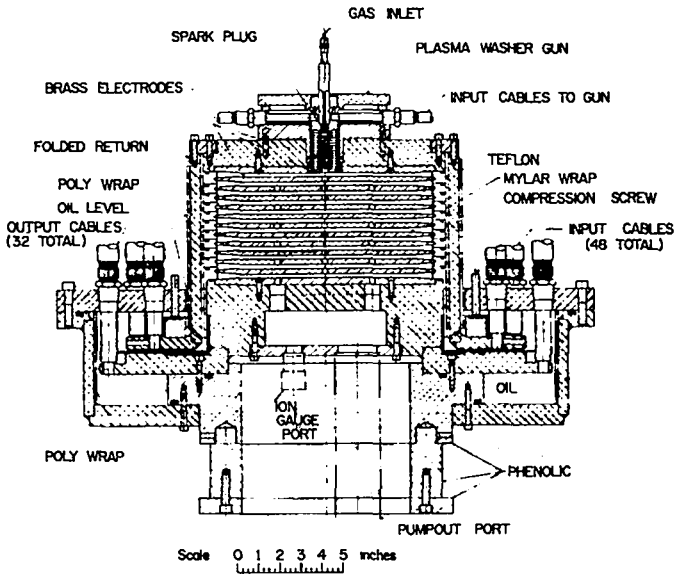

Fig. 5. Diagram of one of the 21 vacuum spark gaps, used to switch the secondary bank of Scylla IV.

plate transmission line (collector plate system) was found to suffer less than 0.02 mm of deflection over its whole area, except at the feed slot of the coil. There the deflection varies linearly with voltage and amounts to 0.96 mm at the full bank voltage of 20 kV, for the clamping arrangement presently in use.[2]

When both the primary and secondary banks are operated in sequence, the switching problem is particularly severe. The primary bank voltage $V_p \approx 50$ kV is applied first, and nearly all of this voltage must be held off by the vacuum spark gaps. The optimum time at which to switch the secondary bank is when V_p has decreased to the voltage V_s to which the secondary bank is charged. This would provide an uninterrupted rise of the coil current in the absence of inductance in the secondary branch of the circuit. If the secondary bank should fire when the primary bank is first switched, it removes a large fraction of V_p from the compression coil and spoils the initial implosion of the pinch.

The secondary-bank spark gaps were essentially identical with one used about 1000 times in the previous Scylla IV experiments[2,3] to short-circuit the coil near the maximum of the current half-wave of the primary bank. The central triggering apertures of the multiple electrodes had a diameter of 6.3 mm, and the gap was embedded in the collector plates. However, when the 21 spark gaps were connected with cables between the secondary bank and the collector plates, the additional voltage caused by doubling of the suddenly applied voltage wave V_p at the open cable ends caused the spark gaps to fire simultaneously with the application of the primary bank.

Rather than make the extensive corrections required to eliminate this voltage doubling, the cure for the prefiring was provided inside the gaps. As shown in Fig. 5, the holes in the 4th and 8th plates were constricted to a diameter of 1.7 mm. It was then found that the spark gaps would stand the application of V_p without breaking down at their operating pressure of ~ 2 mtorr of Ar. They could furthermore be fired at voltages less than 1 kV. It is planned later to modify the gap structure to eliminate the voltage doubling, thereby allowing all of the central apertures to retain their large diameters. In that case the spread of firing times (jitter) of the gaps should be smaller than at present.

In order to minimize the jitter in the firing of the spark gaps, it was necessary to monitor the individual gap currents and to adjust their operating pressures individually. The pressures were adjusted so that the gaps did not fire appreciably before the time at which $V_s = V_p$. After this time, 75% of the gaps fired within a total jitter of about 5 μsec. Under these conditions the decrease in coil current after the first maximum of the component from the primary bank is due to the inductance in the secondary branch of the circuit. This can be seen by

comparing the observed waveform of Fig. 6(b) with the computed form of Fig. 6(c), in which all of the secondary spark gaps are approximated by a single switch with series inductance and resistance.

Plasma Experiments with both the Primary and Secondary Banks

Apparatus

The basic measurements were of relative neutron emission rate and of plasma density and cross-sectional shape as functions of time. The density and shape measurements were made with a 2-m Mach-Zehnder interferometer, illuminated by a cooled, continuously-emitting ruby laser.[3] Time-resolved interferograms were made with a 2.6×10^6 frame/sec, f/4.0, rotating-mirror framing camera,[4] as well as with a three-frame, high-speed image converter. The framing camera allowed measurements to be made for 25 μsec (56 frames) after initiation of the pinch. The measurements reported here were obtained with a mirrorless, 1-m coil at a D_2 filling pressure of approximately 15 mtorr.

Results

The fringe pattern of each interferogram yields $\int n d\ell$ as a function of fringe diameter d_i. Therefore, the total number N of plasma electrons (ions), assuming a uniform plasma density, is closely approximated by $1.26 \times 10^{17} \Sigma_i d_i^2$, where the numerical coefficient is $\pi/4$ times the value of $\int n d\ell$ corresponding to one-half fringe.[2] Typical interferograms are given in Fig. 7 and corresponding graphs of the reduced data showing the fringe shifts vs distance across the discharge tube diameter are given in Fig. 8. These are typical of many discharges in which fairly good simultaneity of firing the vacuum spark gaps was obtained. Graphs of the total number N of plasma electrons vs time are

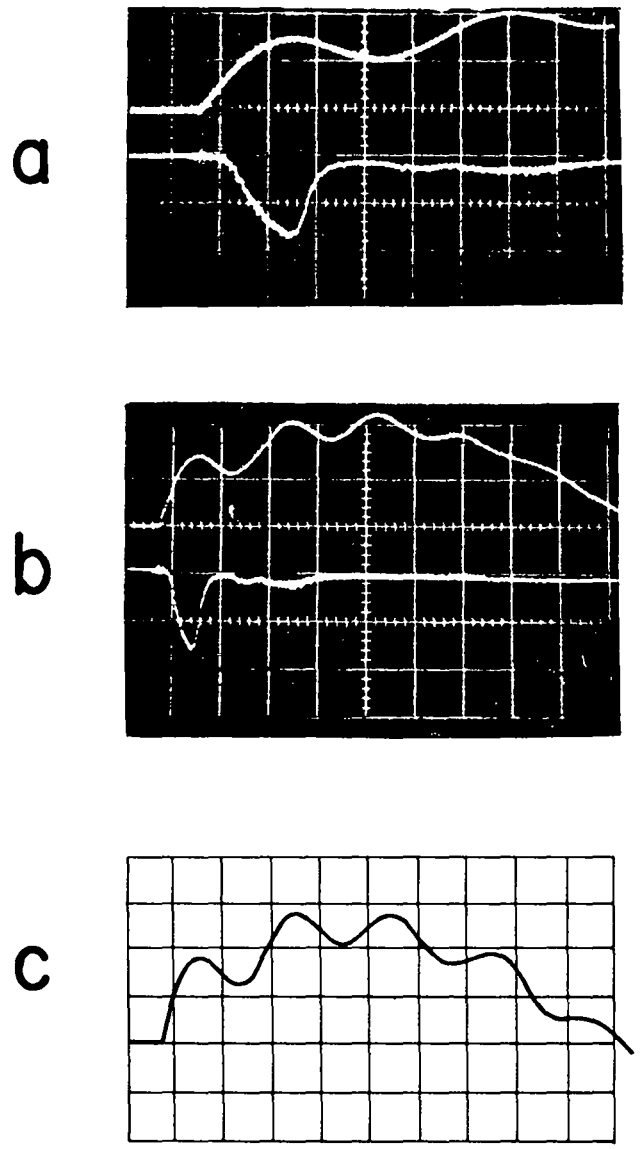

Fig. 6. Waveforms of the compression coil current and the neutron emission rate when both the primary and secondary banks are used. (a) Coil current waveform (upper trace) with V_p = 48 kV and V_s = 15 kV, and the neutron signal (lower trace) from a plastic scintillator. Total neutron yield: 2.6×10^8. Time scale: 2 μsec/div. (b) Same signals as (a) on a time scale of 5 μsec/div. (c) Computed compression coil current waveform using the known circuit parameters, the voltages of (a) and switching the secondary bank into the coil when $V_s = V_p$. Time scale: 5 μsec/div. Vertical scale: 5.1 MA/div.

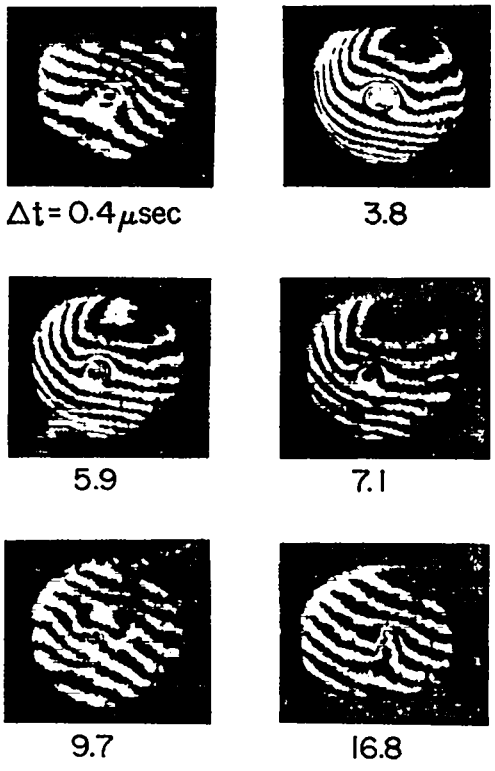

Fig. 7. Interferograms of the Scylla IV discharge corresponding to the current waveform of Fig. 6 with an initial D_2 pressure of 15 mtorr. A few of the 56 photographs taken by the framing camera are shown for illustration and identified by the time Δt after application of the primary bank. Exposure time per frame: 0.42 μsec.

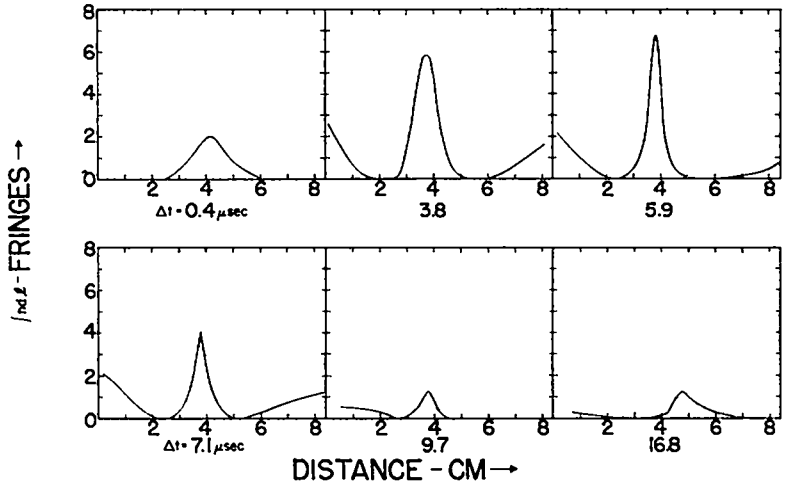

Fig. 8. Graphs of the reduced data of Fig. 7 showing the fringe shifts produced by the plasma vs the discharge tube diameter and identified by the time Δt after application of the primary bank.

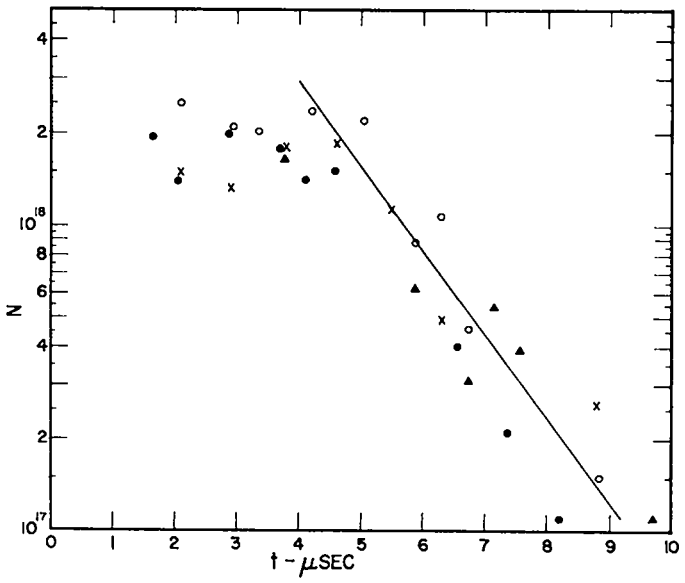

Fig. 9. Total number of plasma electrons vs time for four typical discharges of the primary and secondary banks of Scylla IV. The different symbols correspond to interferometric data obtained on separate discharges. The solid triangular symbols correspond to the current waveform of Fig. 5(a) and (b), the interferograms of Fig. 7, and the reduced data of Fig. 8.

given in Fig. 9. The time variation of N for the central core of plasma is typified by a steady decrease with a characteristic (e-folding) time of ~ 2 μsec. A thin core of plasma is retained for longer times and disappears completely (within experimental error) approximately 17 μsec after initiation of the pinch. At later times there is a distortion of the fringes outside the central region, corresponding to motion of new plasma outside the original core. The plasma core does not show the interchange instability seen in earlier Scylla experiments with short compression coils,[5,6] nor does it drift appreciably during its 17 μsec of existence.

The neutron emission shows an initial rise, as in the experiments with the primary bank alone,[3] and decays to a low level

before the end of the first relative maximum of the current, as shown in Fig. 6(a) and (b). This correlates with the rapid decrease of N. Both phenomena are attributed to end loss.

Discussion and Conclusions

The rapid loss of plasma observed in the foregoing experiments bears out the earlier measurements of rate of end loss made with the primary bank alone.[3] The plasma essentially disappears by the middle of the second half-cycle of the primary component of the coil current. At these longer compression times the interferograms also show the possible effects of cold plasma entering the coil from its ends. This is the interpretation given to the distorted outer fringes at later times in Fig. 7, since the compression time approaches the time for plasma at the preionizer temperature to diffuse into the active coil region. The plasma has more wall contaminant than in the experiments with the primary bank alone, as can be seen by the distortion of fringes near the wall at early times. This is probably because discharges with the large system are much less frequent than those with the primary bank alone, where discharge cleaning is more effective.

---

[1]Kemp,E.L. and Quinn,W.E., Proc. Third Symposium on Engineering Problems in Thermonuclear Research (Berkl,E., ed.) Institut für Plasmaphysik, Garching (1964) p. 70. Also LA-3189-MS (1965).

[2]Jahoda,F.C., Little,E.M., Quinn,W.E., Ribe,F.L., and Sawyer,G.A., J. Appl. Phys. 35, 2351 (1964).

[3]Little,E.M., Quinn,W.E., and Sawyer,G.A., Phys. Fluids 8, 1168 (1965).

[4]Brixner,B., Proc. Sixth International Congress on High-Speed Photography (DeGraaf, J.G.A. and Tegelaar, P., eds.) Tjeenk Willink and Zoon, N.V.-Haarlem (1963) p. 93.

[5]Little,E.M., Quinn,W.E., Ribe,F.L., and Sawyer,G.A., Nuclear Fusion Suppl. Pt. 2 (1962) p. 497.

[6]Little, E.M. and Quinn, W.E., Phys. Fluids 6, 875 (1963).

SCYLLA IV OPERATION

(R.F. Gribble, E.M. Little, N. Lowry, L.H. McDowell, W.E. Quinn)

Investigation of Possible Sustained θ-Pinch Operation

The operation of the Scylla IV device has been studied in a sustained θ-pinch mode. In this mode, the 3-MJ secondary bank would be fired first and the fast primary bank applied in the opposite polarity on the rise of the secondary bank field. The primary bank would be used to reduce the compression coil field to zero or below, where the gas would be preionized. The hot plasma formation would occur on the subsequent sudden rise of the magnetic field. Preliminary computer calculations for the two circuit loops involving the two capacitor banks indicate that this mode of operation is not feasible with the existing experimental arrangement. Figure 10 shows a plot of the coil current vs

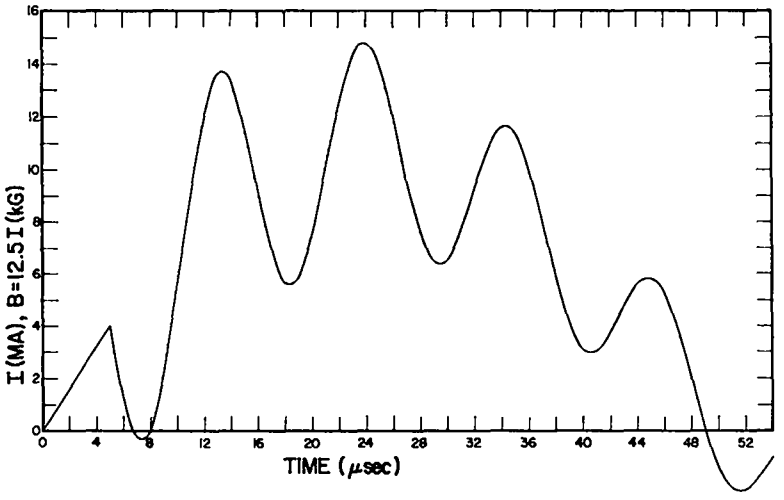

Fig. 10. Coil current vs time in sustained θ-pinch mode.

time. The primary bank is only able to pull the secondary bank field to zero for secondary currents up to 4 MA or for compression coil fields of 50 kG. This limitation exists because the secondary bank is such a large energy sink for the primary bank. The large modulation on the coil current waveform, which results from the energy transfer between the two banks, is quite undesirable.

Power Crowbar Spark Gap Resistive Terminations

An electrolytic resistor has been tested as a possible cable termination for the power crowbar vacuum spark gaps in order to eliminate the voltage doubling, which is presumed to be the source of prefiring of the vacuum spark gaps of the secondary bank (p. 19). An electrolyte of 20 g acetic acid in 100-g of solution, having a resistivity 620 Ω-cm, is being placed into an annular volume between the cable collector electrode on the load side of a vacuum gap and the oil pan ground. This volume has a height of 3.6 cm and a cross-sectional area of 737 cm^2 to give a resistance of 3 Ω with the given acetic acid electrolyte.

The resistive cable termination should completely damp any series resonant voltage effects in the gap and should reduce any voltage doubling at the ends of the cables by 20%. The primary capacitor bank will deposit ~ 1 kJ in the electrolyte of each power crowbar gap while the PCB bank will deposit ~ 2 kJ. This electrolytic resistor is being installed in one of the 21 PCB gaps for tests of the prefiring of the gap. If it is effective in preventing prefiring, a similar modification will be made on the other 20 PCB gaps.

The acetic acid solution has been tested in a smaller 16-Ω geometry with a 0.83-μF capacitor charged to 80 kV. The voltage standoff tests show the liquid to be"quiescent" even with air bubbles on the electrode surfaces. In the 531-cm^3 test volume, 250 kJ were dissipated

in a 2.5-h period with an approximate temperature rise of 5°C. The pulsed measurement, an ac (1 kc/sec) bridge measurement, and e-folding time calculations from the current waveform all give the same resistance value of the electrolyte to within 10%. This indicates that the time response of the electrolyte to the 0.1-μsec pulse is satisfactory.

SCYLLAC PLANS

(Steering Committee)

A committee of Sherwood physicists and engineers has been formed to consider the engineering problems of Scyllac, a toroidal θ-pinch. Scyllac, a closed Scylla, will consist of a 10-cm i.d., 4 m major diam torus. The torus will be fed from the outside having a radial collector plate approximately 30-ft o.d. The system will require over 5 MJ of capacitor energy at 60 kV. Guiding bars and mirror coils may require an equal amount of energy at 50 kV.

The collector will consist of a number of pie sections as shown in Fig. 11. Each section will be held together with through bolts. These bolts will also serve as cable headers to collect the current from the capacitor bank cables, each capacitor having an individual spark gap and six output cables. Figure 12 is a cross section of the through-bolt assembly. A conceptual mechanical design of the Scyllac collector plate was made and its inductance calculated. The energy transfer efficiency of the system was 70%, which is quite close to initial conceptual figures presented in LA-3253-MS.

Committee members are working on several aspects of the Scyllac engineering problems. A 60-kV, 2-μF, reliable capacitor and a low-inductance, high-reliability coaxial cable are being developed. Several types of crowbar switches are being designed and studied and new techniques for cable terminations are being made and evaluated.

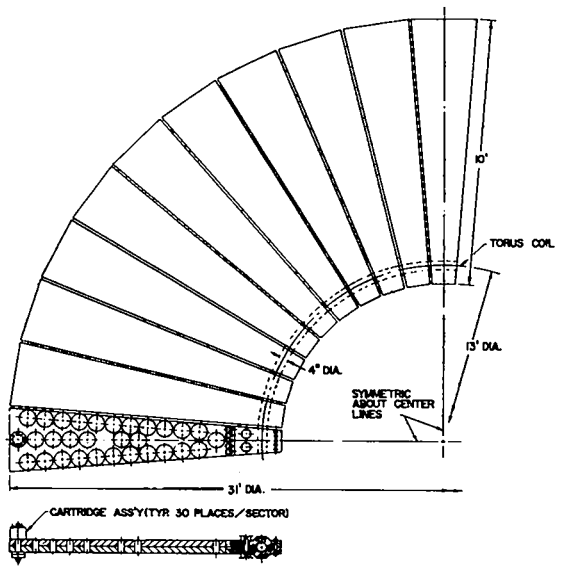

Fig. 11. Section of proposed Scyllac collector.

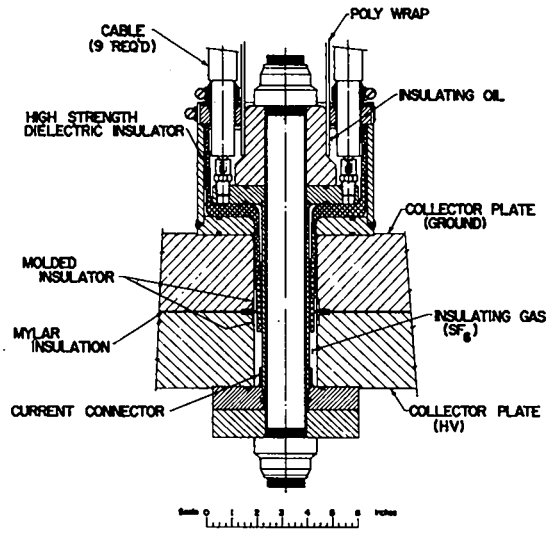

Fig. 12. Cross section of through-bolt assembly.

A two-pie sector of Scyllac will be designed, installed, and operated. This sector will be used to evaluate all new components, designs, and engineering techniques for Scyllac.

SCYLLA IV CURVED SECTOR EXPERIMENTS

(W.H. Borkenhagen and W.E. Quinn)

Preparations are being made for experimental plasma studies in curved sectors of a torus on the Scylla IV device to test various stabilizing techniques for overcoming the outward drift of the plasma due to the radial magnetic field gradient (cf. LA-3289-MS). A basic design of a multipole-bar sector arrangement has been worked out in sufficient detail to determine the various mechanical and electrical problems. The basic design is applicable to curved sectors with radii of curvature in the range of 1.5 to 2.5 m, as well as to straight sectors and to various multipole bar arrangements. In addition, the design accommodates a narrow single-turn coil in the regions between curved sectors where the multipole bars are fed. This loop, energized from a separate capacitor bank, can be used either to make a magnetic mirror region between sectors or to maintain the homogeneity of the axial magnetic field.

The individual coil sectors will have a length of approximately 25 cm as dictated by specific multipole arrangements to produce the desired magnetic field geometry. Such coil sectors will be separated by approximately 5 cm to provide the required space to bring in the current feeds to the multipole bars which will lie inside each coil sector and parallel to the sector axis. Located between the current feeds to adjacent coil sectors will be the narrow, single-turn loop coil.

The coil sectors will be energized from the existing Scylla IV machine. A capacitor bank platform extension will accommodate

~ 280-kJ of 50-kV energy storage to energize the multipole bars and loop coils. The cables (improved type RG 17/14) from the capacitor spark-gap units will connect into 12-cable cartridge units with a through bolt design into horizontal collector plates located above and to the side of the coil sectors. Each horizontal collector or parallel plate transmission line will make a 90° bend into the vertical plane and feed down and into a slot between the coil sectors transverse to the axes of the latter. The multipole bars will connect to these parallel plate current feeds. The ends of the multipole bars at the opposite end of the sector will be taken out into the sector slot and appropriately connected together. The loop coils will be fed in a similar manner.

The multipole bars in each coil sector will be vacuum potted with epoxy and glass fiber in a cylindrical shell and as an integral unit with the parallel plate current feed which extends into the coil slot. The potted section of the parallel plate current feed will terminate in a current joint approximately 15 cm beyond the outside diameter of the sector coil. The epoxy-glass fiber arrangement will provide both the electrical insulation and mechanical support for the bars. Various types of multipole bar units, made in such integral potted units, can be inserted into the sector coils and connected to the parallel plate collector system. The latter system will be mounted on a track below the platform to allow it to be retracted with the connected cables from the coil regions to facilitate the assembly of coil sectors and bar units.

It is to be noted that a certain flexibility exists for experimenting with various multipole bar arrangements, provided the individual bar geometries are adaptable to a uniform circular bore in the sector coils.

A tentative design of the loop coil has been made, which also incorporates an epoxy-glass fiber arrangement for mechanical support and electrical insulation.

POSSIBLE SINGLE-TURN MIRROR INSERTS FOR SCYLLAC EXPERIMENTS

(D.A. Baker, R.F. Gribble, W.E. Quinn, F.L. Ribe)

In the original Furth-Rosenbluth,[1] $\ell = 0.2$ method for stabilizing a low-β torus it is essential to have magnetic mirrors at the junctions where the quadrupole currents reverse sign. Even in the $\ell = 0.3$ method, suggested recently by Furth (personal communication), it is desirable to have current loops act as "guard rings" at the current-reversing junctions, in order to overcome outward bending of the B_z lines into those gaps of the main, θ-pinch coil which are necessary to accommodate the current feeds to the multipoles. Accordingly, an investigation was made of the capacitor energy necessary to drive such current loops and to determine the effects of inductive coupling to the main coil. A crucial parameter is the voltage necessary to drive the loops in order that their rise time be nearly equal that of the main B_z field, taking account of the back emf induced by the latter in the loop.

As a first step, the flux lines in a practical arrangement of conductors with complete skin effect were investigated. The arrangement, shown in Fig. 13, shows one-half of a periodicity length (no curvature) with half of the single-turn coil 2 at the center and half of the sectored, main compression coil 1 with realistic dimensions. Using a resistance analog board,[2] a gap of 2 cm between coils 1 and 2 was found necessary to allow sufficient return flux to provide a mirror ratio of 1.4 on the axis at a minimum current ratio 1:3 between coils 2 and 1. From the board the following inductances were found: $L_{12} = M = 21$ nH (coupling coefficient $k = 0.29$). The current I_1 necessary to generate 90 kG in

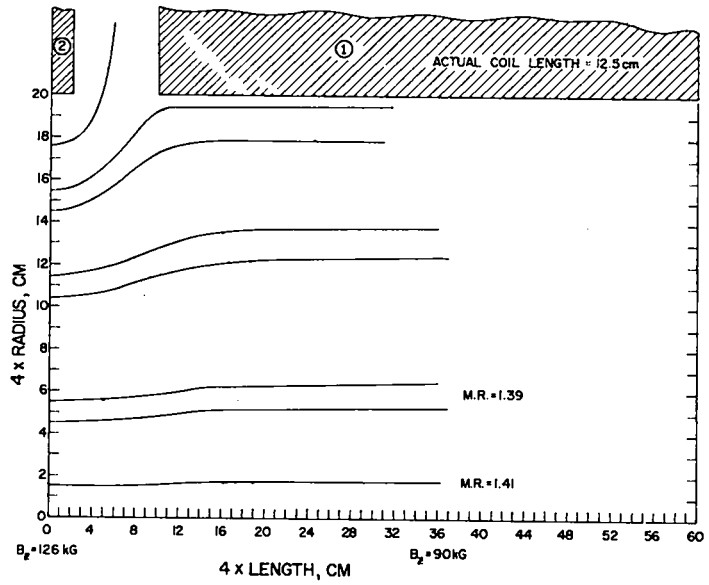

Fig. 13. Flux lines in arrangement of conductors with skin effect.

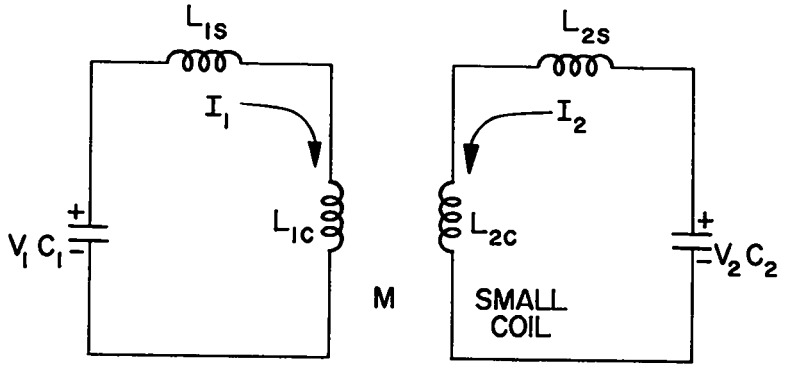

Fig. 14. Coupled-circuit problem.

the center of coil 1 is 1.7 MA. Following earlier estimates[3] for a full-scale Scyllac, the desired period of the system is taken to be 12 μsec.

In order to check the time dependence and magnitude of the currents, the coupled-circuit problem of Fig. 14 was run, using the crowbar code[4] and the following parameters: V_2 = 54.7 kV, C_2 = 19.8 μF, L_{2S} = 0.024 μH, L_{2C} = 0.160 μH, M = 0.021 μH, V_1 = 44.6 kV, C_1 = 72.7 μF, L_{1S} = 0.0172 μH, L_{1C} = 0.033 μH. Here L_{1S} and L_{2S} are leakage inductances associated with compression-coil and loop circuits. In the code both circuits were closed at t = 0. The currents are seen to peak sufficiently near to each other, although they become progressively more out of phase on the second half-cycle. This would not matter in the crowbarred case, where only the first quarter-cycle of the variation shown in Fig. 15 is used. The ratio of capacitive energies is

$$(1/2)C_2V_2^2/(1/2)C_1V_1^2 = 0.41.$$

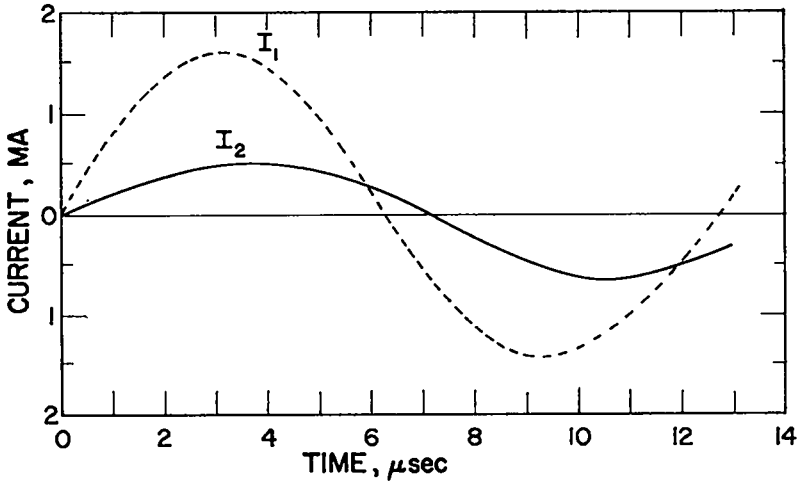

Fig. 15. Current variation with time.

For reference, the analytical solution for the currents of Fig. 14 may be presented. Here $L_1 = L_{1S} + L_{1C}$ and $L_2 = L_{2S} + L_{2C}$.

$$I_1(t) = \{[V_1/C_2\bar{\omega}_1 - (V_1L_2 - V_2M)\bar{\omega}_1] \sin \bar{\omega}_1 t - [V_1/C_2\bar{\omega}_2 - (V_1L_2 - V_2M)\bar{\omega}_2] \sin \bar{\omega}_2 t \} / (L_1L_2 - M_2)(\bar{\omega}_2^2 - \bar{\omega}_1^2).$$

L_2 is given by the same formula with the subscripts interchanged. The natural frequencies are

$$\bar{\omega}_1 = [\omega_1^2 + \omega_2^2 + \sqrt{(\omega_1^2 - \omega_2^2)^2 + 4k^2\omega_1^2\omega_2^2}\,]^{\frac{1}{2}} / \sqrt{2(1-k^2)}$$

$$\bar{\omega}_2 = [\omega_1^2 + \omega_2^2 + \sqrt{(\omega_1^2 - \omega_2^2)^2 + k^2\omega_1^2\omega_2^2}\,]^{\frac{1}{2}} / \sqrt{2(1-k^2)}$$

where

$$\omega_1^2 = 1/L_1C_1 \text{ and } \omega_2^2 = 1/L_2C_2$$
$$k = M/\sqrt{L_1L_2}.$$

For $\omega_1 = \omega_2 = \omega_0$,

$$\bar{\omega}_1 = \omega_0/\sqrt{1-k} \text{ and } \bar{\omega}_2 = \omega_0/\sqrt{1+k}.$$

---

[1] H. P. Furth and M. N. Rosenbluth, Phys. Fluids 7, 764 (1964).

[2] K. E. Wakefield, NYO-7312 (1956).

[3] W. E. Quinn, F. L. Ribe, W. B. Riesenfeld, G. A. Sawyer, and J. L. Tuck, LA-3289-MS (1965).

[4] D. A. Baker and L. W. Mann, LAMS-2435 (1960).

ANALOG SOLUTION OF MULTIPOLE STABILIZING CONDUCTORS

(G.A. Sawyer)

Resistive paper with uniform resistivity can be used for analog solutions of magnetic fields in the x-y plane of rectangular coordinates to give the components of magnetic field B_x and B_y produced by z-directed currents. It can be easily shown by vector analysis that the real magnetic field configuration and the analog field fulfill the same vector equations and, in particular, Laplace's equation. The solution is similar to that of the resistor board for cylindrically symmetric problems. Electric potential V on the resistive paper is the analog of the magnetic vector potential A_z.

The resistive paper analog has been used previously in the LASL Sherwood program for solution of similar problems. Recent refinements have considerably improved the accuracy so that gradient of magnetic field can be measured. The refinements include addition of stable power supplies, better voltmeters, and a differential voltage probe which measures $\partial V/\partial x$ directly.

Several problems on quadrupole fields in Scyllac have been run on the analog to determine what conductor geometry would have the best electrical characteristics. The analog readily measures inductance of a conductor configuration and the gradient of magnetic field (a measure of quadrupole strength). Thus, it is possible, by trial and error, to approach geometries producing maximum quadrupole strength for minimum energy expended.

Figure 16 summarizes results on quadrupole conductors in a Scylla coil. Both asymmetric, three-conductor and symmetric, four-conductor cases have been treated. The conductors were always spaced 0.79 cm from the Scylla coil and were 0.63-cm thick with their inner surfaces on a 10-cm diam circle. The figure gives (1) total inductance of the bar system, (2) the gradient of magnetic field at the center of the Scylla coil per kA of driving current - a measure of quadrupole strength, (3) column two divided by inductance per unit length - a measure of quadrupole strength per unit magnetic energy, and (4) the magnetic field strength at the surface of the quadrupole conductors on the side toward the Scylla coil - a measure of magnetic pressure on the bar.

It is clear that conductors imbedded in recesses in the Scylla coil produce a weak quadrupole field and have relatively high inductance. Broad straps (the last cases shown), with strap width equal to spacing between straps, have both low inductance and high quadrupole strength and are the best cases considered so far.

Results given here are confirmed by measurements made by G. Boicourt at LASL on an actual three-dimensional model of current conductors.

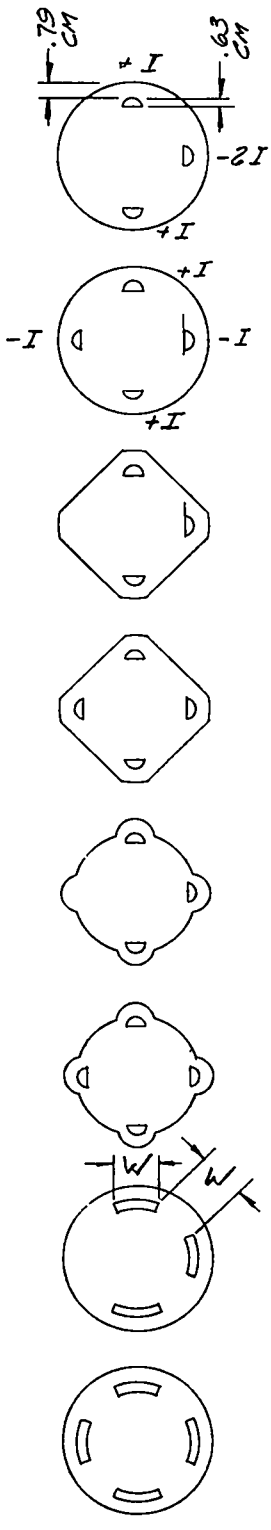

1	2	3	4
L_{total} (nH/cm)	Grad B (G/KA-cm)	Grad B/L (G/KA-cm-nH)	By(bar) (G/KA)
4.0	6.48	1.6	430
2.7	5.72	2.1	240
3.57	5.36	1.50	415
2.41	5.37	2.22	215
3.19	3.90	1.22	370
2.20	2.92	1.32	170
1.84	5.1	2.76	170
1.22	4.9	4.00	92

Fig. 16. Analog solution for quadrupole conductors in a Scylla coil.

SCYLLACITA, A SMALL THETA-PINCH MACHINE

(E. Dolnick, R. Dike, E. Kemp, and G.A. Sawyer)

The staffs of both Project Sherwood and Group GMX-6 at LASL are interested in explosively imploding a θ-pinch. The maximum field should increase to over 500 kG with explosive compression, increasing the neutron yield by two or more orders of magnitude. It was agreed that Sherwood would build a compact Scylla-like θ-pinch machine that could be installed at a GMX-6 firing site. Scyllacita is the name given to the θ-pinch machine to be used for this purpose.

Scylla θ-pinches require large θ voltages (~ 1 kV/cm) around the coil, short rise times (2-5 μsec), and maximum fields of 75-100 kG. These were the design criteria for Scyllacita. The capacitor and switch designs are the essence of low-inductance, fast rise time systems. Scyllacita uses 24 capacitors of 14 μF and 20 kV, each with its own three-element spark gap. Figure 17 shows a schematic of the gap mounted to a low-inductance (< 20 nH) capacitor. The measured inductance of this assembly, with the 12 cables shorted at the header, is 31 nH.

A schematic of the system is given in Fig. 18. Two capacitor-gap assemblies are charged in parallel and switched into series when the gaps are fired. This provides essentially twice the dc voltage for the pulse voltage on the load. The 12 cables from each capacitor are interconnected in the "mix header," the braid of S-2 cables being pulsed up to the dc charge voltage of the S-1 capacitors. Two 27-cm long coils have been used; a straight bore, 8-cm-i.d. coil, and a similar

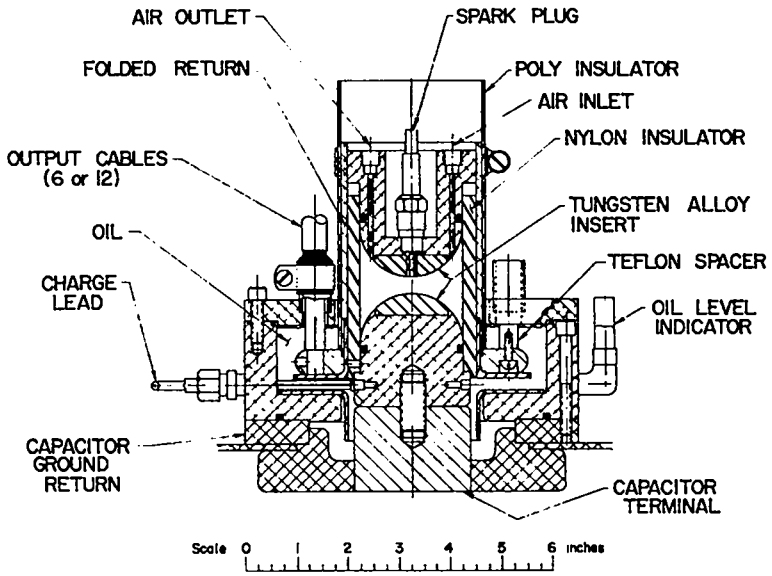

Fig. 17. Three-element spark gap mounted to low-inductance capacitor.

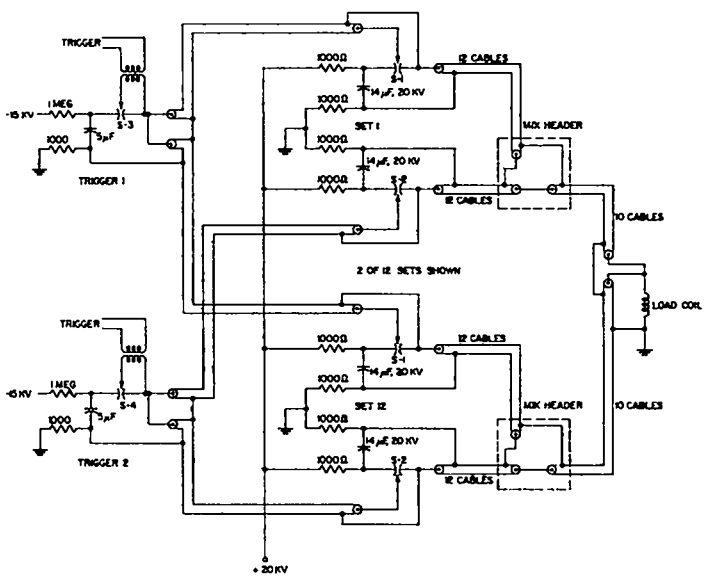

Fig. 18. Schematic of low-inductance, fast-rise system.

one with mirrors. The following table gives the system dynamic characteristics using the straight coil and charging the bank to k8-kV dc.

C	= 86.4 μF	Transfer Efficiency	= 59%
V	18 x 2 = 36 kV	$\tau/4$	= 2.9 μsec
W	= 56 kJ	I_{Max}	= 1.65 MA
V_θ	= 21 kV (835 V/cm)	B_{Max}	= 75 kG

Scyllacita has consistently produced 10^6 to 10^7 neutrons on the second half-cycle of magnetic field with the straight coil. First half-cycle neutrons have also been produced by connecting one set of the capacitors to a separate firing set and firing it first. Then the main bank is fired at the second field reversal of the preionizing bank, thus trapping a reversed field in the plasma. The machine will produce 10^6 neutrons in this mode although with less consistency. The x-ray temperature was 330 eV as measured by the dual absorber technique.

The straight coil is being used because the explosive compression experiment will have this type of coil. Various warm-up procedures to condition the discharge tube are being investigated. Some smear pictures will be made of the plasma and actual implodable coils will be tested before the machine is installed at the firing site.

SCYLLA I LASER EXPERIMENTS

(P.N. Mace and G.H. McCall)

Aluminum mirrors of 120-cm radius of curvature have been mounted at the ends of the Scylla I discharge tube to create a laser cavity. Spectroscopic measurements have been made with the mirrors aligned and unaligned on Ne, Ar, N_2, CO_2, and Kr discharges. Strong evidence of optical gain (with possible laser action) has been observed at 41 wavelengths, with a possibility of gain at another 41 wavelengths. Spectroscopic measurements were made over a total of from 20 to 40 shots, for two reasons: (1) the intensity of the lines is too low to give good data on a one-shot basis; (2) using a large number of shots tends to average out shot-to-shot variations in the plasma characteristics, thus giving the data more validity.

Most of the data have so far been taken with a Hilger medium quartz spectrograph. This instrument is useful in looking over a very wide wavelength range (2,000-10,000 Å), but has low resolution. A better instrument, a McPherson 1-m grating spectrograph is now in use. It provides a dispersion of about 7.6 Å/mm, first order. A working resolution of 0.07 Å has been obtained using a very bright source; in these experiments a wider slit width will be necessary due to low source brightness, reducing the resolution somewhat. Time histories of individual lines can be obtained by using a photomultiplier in conjunction with an output slit.

Figure 19 is a portion of the microdensitometer trace of data taken from a Kr plasma, and indicates the type of result being obtained. Going from the left of the figure, lines one and three are designated as having a very high probability of optical gain due to the resonant cavity; line two shows a moderate (or questionable) probability of gain; lines four, five, and six indicate no gain over the unaligned condition.

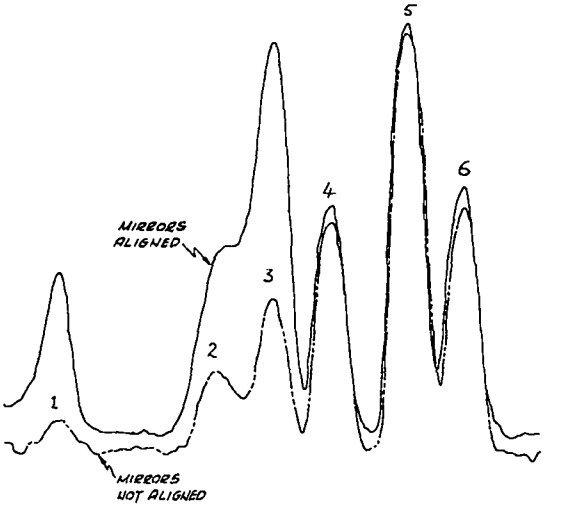

Fig. 19. Part of typical microdensitometer trace of spectrum from a Kr plasma.

All data were taken at initial gas pressures of from 2.5 to 5.0 μHg, which are considerably lower than the pressures normally used in Scylla. The reasons for using low pressures are twofold: first, the apparent laser transitions seem to disappear, i.e., show less evidence of change over the unaligned condition, at higher pressures. This may be due to Doppler broadening of the lines, reducing the gain. Second, for low-pressure operation, at pressures of 10 μ or more, the end windows are rendered effectively opaque in one or two shots, and a high-intensity continuum radiation obscures the line transitions on time integrated spectra.

Already differences between these results and the results of other workers can be noted; in general, the apparent laser transitions obtained are not those seen previously. The reasons for this are not yet

known; it may be that higher order transitions are involved. Another striking difference is that whereas other researchers have found that the strongest laser lines are also the strong lines observed in spontaneous emission,[1] the case here seems to be rather the opposite (e.g., Fig. 19).

A longer coil is being installed on Scylla I to give a longer discharge with consequent higher gain. This, together with improvements in the optical system, should give greater enhancement.

---

[1]Bridges, W. B., and Chester, A. N., IEEE J. of Quantum Elect., QE-1, No. 2, 66 (1965).

TEST OF GIANT-PULSE RUBY LASER FOR SCATTERING EXPERIMENT

(T. Langham, A.S. Rawcliffe, F.L. Ribe, D. Steinhaus, K. Thomas)

A 50-MW, giant-pulse laser (modified K1-Q) has been delivered by the Korad Corporation and was tested to see if specifications are met. The giant-pulse arrangement consists of a Pockels cell with Brewster-angle, glass-plate polarizers, a passive Q-spoiler consisting of a cell filled with cryptocyanine in methyl alcohol, and a sapphire end-reflector with Fabry-Perot modes spaced by 0.44 Å. Some difficulty was experienced with the solid state electronics of the Pockels-cell (p-c) circuit. The silicon-controlled rectifier controlling the p-d trigger pulse was faulty and was replaced. Simultaneously the polarity of the pulse was reversed by modification of the SCR circuit.

In order to measure its line-width, the laser was operated at a 35-ft Wadsworth spectrograph. Using a slightly damaged ruby furnished by the manufacturer, the laser beam was directed at a white disc from which a portion of the reflected light was focussed by a mirror on the spectrograph. Two exposures, one discharge each, of the 6943-Å line with 2-μ slit width, are shown in Fig. 20. For the lighter exposure an ND-1 filter was used. The laser output was monitored by a photocell in light transmitted through the disk.

The next step of the test is to place a new ruby in the laser and to attempt to adjust the cryptocyanine concentration until the satellite of Fig. 20 (spaced by 0.44 Å) is gone or minimized. When this was attempted, the laser ceased to function. The difficulty was found to

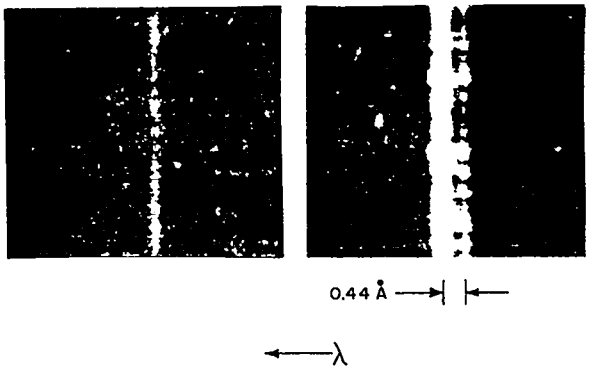

Fig. 20. Exposures of the 6943-Å ruby laser line.

reside in the Pockels cell which had somehow degraded so that its presence prevented the laser from operating. This cell was sent back to Korad and replaced.

The original, pitted ruby was also sent back to Korad for repair. Upon its return, it was placed in the laser, which was found to operate satisfactorily. The output was examined with a McPherson 1-m focal length spectrograph and, with the proper concentration of passive dye, was found to consist of a single line whose width was less than the instrumental width of the spectrograph ($\sim$ 0.1 Å).

FABRY-PEROT MONACHROMATOR FOR SCATTERING EXPERIMENT

(F. L. Ribe, K.S. Thomas)

The 3-etalon instrument referred to in LA-3320-MS, p. 94, has been fabricated and fitted with pressure-scanning instrumentation. A pair of $\lambda/100$ plates of small diameter was installed in an etalon holder with a 15-mm spacer and the fringes recorded photoelectrically as the chamber pressure of SF_6 was varied. At $\lambda = 6328$ Å the SF_6 index of refraction was found to be 7.2×10^{-3} greater than unity. A free spectral range of 6 Å in the final instrument can therefore be scanned with a pressure range of 17.6 psi.

The three pairs of 50-mm etalons have been ordered through Industrial Optics, Inc. They have been fabricated in England and tested by Profs. J. Mack and F. Roessler at the University of Wisconsin. Their flatness is better than $\lambda/150$ before soft coatings are applied. The plates are now back in England for application of the spacers (respecified as 0.4 mm) and the soft coatings.

HYDROMAGNETIC PLASMA GUN PROGRAM

(I. Henins and J. Marshall)

Introduction

The work reported in the last semiannual report (LA-3320-MS) has been continued and a report containing a rather complete summary of this work with the understanding of the results was presented at the 1965 IAEA Conference on Plasma Physics and Controlled Nuclear Fusion Research at Culham, England. Although this paper contains material found in previous semiannual reports, for completeness it is reproduced with only a minor deletion.

Future plans for the gun program include an effort to increase both the quantity and energy of the fast plasma output. A gun of higher voltage (50 kV) is at present being designed for this purpose.

THE FAST PLASMA FROM A COAXIAL GUN*

John Marshall and Ivars Henins

Abstract

An investigation of the phenomena accompanying the acceleration of the fast plasma from a coaxial gun has been made using a variety of techniques including particle analysis, electric probing, space current

*This section (pages 48 through 67) is reproduced without any editorial changes except for adjustment in the figure numbers to correspond with those in the other parts of this Semiannual Report.

probing by Rogowsky loops, diamagnetism as measured by external pickup loops, high speed photography both directly of the discharge between the gun electrodes and indirectly by the light of the secondary plasma produced when the fast plasma strikes a target. The gun is normally operated with an axial bias magnetic field between the electrodes. The fast plasma injected into a guide field contains $\sim 5 \times 10^{17}$ deuterons with a wide spread of energy peaking around 8 keV. It is generated over a period of slightly more than 1 μsec, beginning 2 μsec after first breakdown. When the gun is fired into a field free region, the production of the fast plasma appears to be consistent with a model based on the expansion of a fully ionized magnetized moving plasma into vacuum. Such a model would predict that a large fraction of the magnetic and streaming kinetic energy of the moving plasma between the gun electrodes would appear as kinetic energy of the front part of the plasma. The acceleration of the plasma is a gradual one over a distance of 50 cm or so beyond the gun muzzle. When the gun is fired into a 16-kG axial guide field the acceleration process is localized to a region within a few cm of the gun muzzle, the ions and electrons enter the guide field by separate processes and by different paths. The detailed acceleration mechanism is still not understood.

1. Introduction

This paper is an attempt to describe and, as nearly as possible, to explain the phenomena responsible for the acceleration of the fast component of the plasma from a coaxial gun.[1,2] It must be emphasized that this is one particular gun, and that another coaxial gun may differ violently in its characteristics. The differences depend on details of design and on adjustment of easily variable parameters, which are optimized according to the immediate objectives of the experimenter. The gun discussed here is the result of a parameter search in which all gun dimensions except inner electrode diameter were optimized for the production

of thermonuclear type deuterium plasma. The yield was judged by the number of neutrons produced when the fast plasma was directed against a strong magnetic mirror. Target neutrons produced when deuterons strike the walls of the system are distinguishable from these neutrons and were excluded from consideration. The reason is that optimization on target neutrons tends to lead to a different mode of gun operation and a completely different set of parameters. Contamination of the fast plasma by impurities either of other ions than deuterium or of slow deuterium plasma was not considered in the optimization procedure so long as it didn't interfere with neutron yield. Later, however, changes have been made in gun design which were intended to reduce such contamination, and which are believed to have done so. In addition the gun is now operated with an axial bias magnetic field, since this was found to improve the quality of the fast plasma. Regretably the more inflexible gun parameters have not been reoptimized after these changes because of the large amount of effort required.

2. Gun Design and Operating Parameters

The gun design is shown in Fig. 21. The electrodes are of copper. The axial variation of the bias field is shown in Fig. 22. It is pulsed on by a large diameter coil surrounding the gun barrel. Timing is such that the bias field has soaked through the outer gun electrode, and the field external to the barrel due to the coil is small at gun firing time. The gun bank has 30-μF capacity and is normally charged to 21 kV. It is switched by 6 ignitrons through 36 low inductance cables and as seen from the terminal end of the gun electrodes has about 10 nH inductance. A purposely inductive electrolytic resistor is connected across the gun terminals to dissipate energy safely in case of an ignitron prefire, but so as not to interfere significantly with terminal voltage during approximately the first 2 μsec. The fast valve is operated by thermal expansion of a short section of mechanical transmission line, which is heated by about 50°C in 10 μsec by current from a

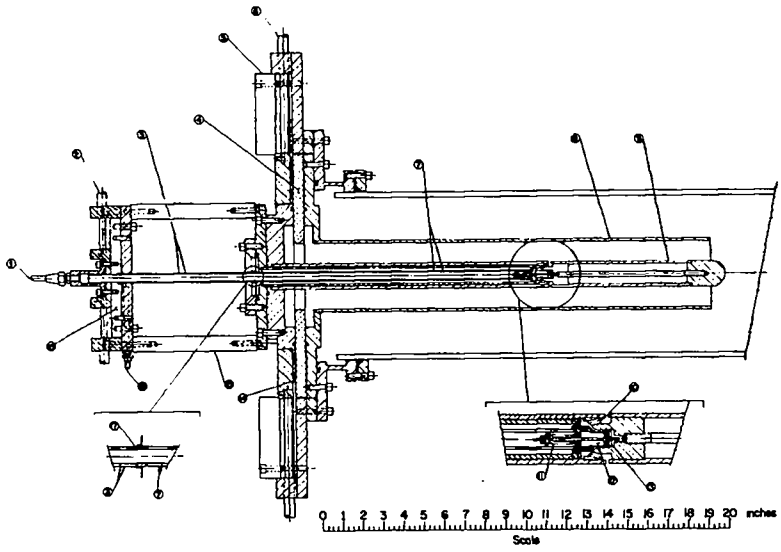

Fig. 21. 1. Gas inlet. 2. 16 Rex 4 cables to valve driver capacitor bank (240 μF, 2kV). 3. Driver section (2 coaxial 0.25-mm wall Inconel-x tubes). 4. Glass insulator. 5. Lucite clamping ring. 6. 36 B.I.C.C. type 20 cables to gun capacitor bank (30 μF, 21 kV). 7. Sonic line. 8. Copper outer electrode. 9. Copper inner electrode. 10. Gas outlet holes (15 holes, 3-mm diameter). 11. Valve spring. 12. Valve plenum. 13. Teflon bumper washer. 14. Polyethylene insulation. 15. Phenolic insulator. 16. Cooling air inlet. 17. Small holes for air outlet.

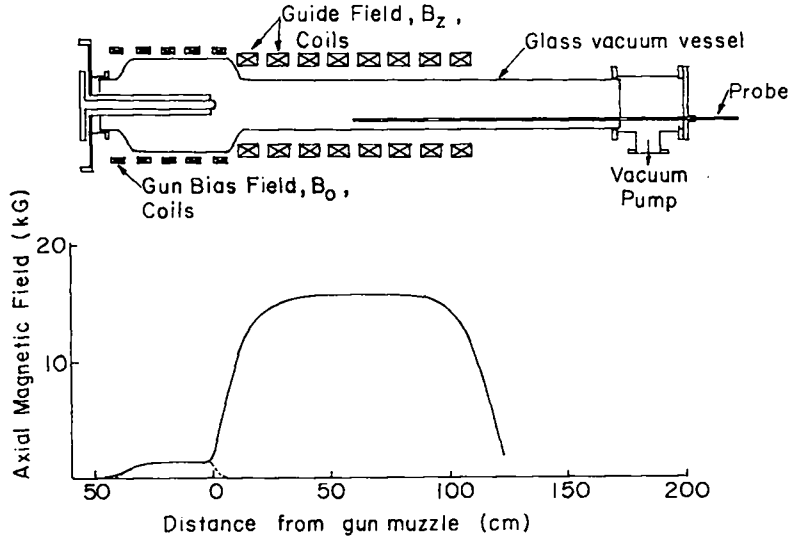

Fig. 22. Experimental arrangement and axial magnetic field strength.

low energy auxiliary capacitor bank. Approximately 1-cm^3 atm of deuterium gas is introduced by the valve through a labyrinth, which prevents erosion of the valve gasket by the plasma and consequent introduction of impurities, but which also slows down gas admission and therefore affects the distribution of gas density at gun firing time. This is probably the only significant mechanical design change made after parameter optimization.

3. Gun Barrel Phase

It appears that gun operation can be considered as consisting of two separate subsequent phases. The first one, the gun barrel phase, lasts from first breakdown until current appears at the muzzle. This requires about 2 μsec. Before the gun bank is triggered enough time delay has been allowed after gas admission to provide a substantial gas density throughout the gun barrel, from terminals to the space just beyond the muzzle. Apparently the gas density near the gun terminals has an optimum value, large enough so that a discharge can form in this low inductance region, dense enough so that in being driven toward the muzzle a large amount of kinetic energy of streaming plasma can result, but tenuous enough that it can be driven to high velocity and so absorb energy. The yield of fast plasma appears to depend on the amount of energy which can be stored in the first part of the discharge in the magnetized streaming plasma inside the gun barrel. The front of the radial discharge moves through the deuterium gas between the electrodes at a roughly uniform speed of about 2.5×10^7 cm/sec. The resulting plasma is not snowplowed ahead of the current front but is left behind, moving at a lower speed than the front and still carrying some radial current. The gun terminal current in the meantime is rising almost linearly (Fig. 23), so that by the time the current front reaches the muzzle the terminal current is about 2.7×10^5 A about three-fourths of which is being carried by plasma behind the front. Fast plasma is emitted by the gun only after the current front has reached the muzzle.

Violent electric and magnetic phenomena take place there while it is being emitted but are not apparent in the current and voltages measured at the terminals. The fast plasma carries 1000 J or more of kinetic energy, a substantial fraction of the energy delivered electrically to the gun terminals before its emission. Its speed is much larger than the speed of the plasma behind the current front, and three or four times the speed of the current front itself. It appears then that it is accelerated by some phenomenon at the muzzle which is driven by energy stored during the gun barrel phase. Differences within reasonable limits in the gun barrel phase produce quantitative but not qualitative differences in the fast plasma acceleration phenomenon. It appears that, if conditions at the gun muzzle remain substantially the same, the speed and energy content of the fast plasma will depend on the amount of energy stored in the gun barrel phase and on the azimuthal uniformity of the gun barrel discharge when it reaches the muzzle but that the acceleration mechanism will not change essentially.

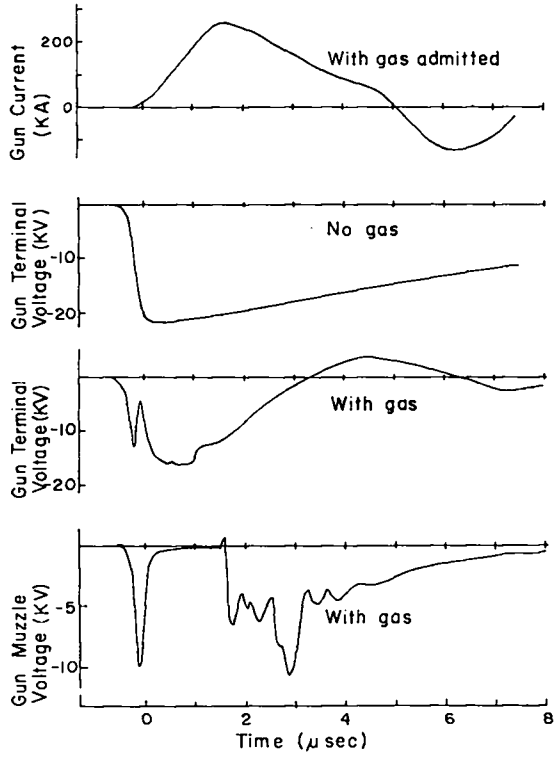

Fig. 23. Time variation of gun current and voltages. Gun muzzle voltage measured with probe touching tip of center electrode.

The exact role of the gun barrel bias field is not understood. It is known to affect the breakdown conditions, allowing the gun to be fired at lower gas pressures, and to have a different optimum time delay after gas admission for production of fast plasma ($\sim$ 245 μsec without B_0, $\sim$ 330 μsec with B_0). With bias field the fast plasma is somewhat faster

than without and there is considerably less late diamagnetism observed in the guide field beyond the muzzle. The most likely implication of this is that there is less slow plasma injected into the guide field. The slow plasma is assumed to be to a large extent, the streaming plasma behind the current front in the gun barrel. In the case of zero bias field it is observed to account approximately for the amount of deuterium admitted by the valve. The amount of slow plasma with bias field is unknown.

The amount and energy of fast plasma produced at the gun muzzle appears to depend on the gas density distribution in this region at gun firing time as well as on the density along the gun barrel. A high muzzle density leads to a lower particle energy in the fast plasma, perhaps simply because more mass is present to share the available energy. The gas density distribution along the gun barrel and at the muzzle were optimized as well as could be by varying the position of the gas inlet, the amount of gas admitted and the delay after gas admission. Most likely a better gas distribution is possible, but it will be complicated to achieve.

4. Magnetized Plasma Expansion Model

A model which may be capable of explaining partially the generation of fast plasma at the gun muzzle is simply the expansion of the moving magnetized plasma between the electrodes of the gun barrel into the evacuated space beyond the muzzle. The presence of the azimuthal magnetic field in the plasma, which is due to the axial current along the center electrode and along the current jet extending out in front of the center electrode, tends to make the plasma behave like a continuum, and allows pressure to be transmitted from one part to another at Alfvén speed, which may be faster than ion thermal speed. Alfvén waves in the expanding parts of the plasma will be expected to have

Alfvén velocity relative to the moving plasma so that expansion will not be limited to this speed. On the other hand the expansion process will be slow for speeds much greater than the Alfvén velocity. The process would be relatively simple for a one dimensional expansion (plane surface separating magnetized plasma from vacuum), and could presumably be calculated from known initial conditions. Here one would expect all magnetic and thermal energy to be transferred eventually to streaming energy with the particles near the edge of the plasma having a much larger energy than those deep inside.

This model has serious deficiencies when applied to the coaxial gun in that the radius of the gun is about of the same size as the gyro radius of the fast plasma ions in the magnetic field of the muzzle current. This makes the behavior of the ions highly non-adiabatic, so that they cannot be considered to be attached to field lines as is required by the model. The situation is further complicated by the non-uniform azimuthal magnetic field in this case, and the three dimensional expansion to be expected. For these reasons it would appear to be a fruitless endeavor to attempt to solve the expansion problem for this case. Qualitatively the model may have some value, however, particularly since the expansion might be expected to take place mostly in the axial direction where the large field gradients might be expected to be found at the front of the current jet, and incidentally this is the direction in which the fast plasma is observed to emerge.

The expansion of magnetized plasma away from the gun is equivalent to the emergence of a jet of current together with the plasma necessary to carry it. In any case, flux is transported from between the gun electrodes into the space beyond the muzzle and a voltage between the electrodes is implied. The voltage can be thought of either as the $\vec{v} \times \vec{B}$ type generator emf of the emergent magnetized plasma stream or as the voltage required to account for the rate of flux emergence, the two pictures being equivalent. The voltage between the gun electrodes is of such a direction as to drive a plasma continuation of the axial current along

the electrodes. As the magnetized plasma expands, the magnetic field decreases even in the case of a perfectly conducting plasma, and the current carried by the jet beyond the gun muzzle falls off with distance. The E/B field line or plasma speed, resulting from the crossed radial electric field and azimuthal magnetic field of the current jet, can only increase if a sample of plasma is followed in its motion away from the gun muzzle. Non-adiabatic effects having to do with large gyro radii of ions can distort this seriously so that a local $\vec{E} \times \vec{B}$ direction can actually be opposite to the streaming motion of ions.

5. Experimental Observations

A number of different kinds of measurements have been made in the region beyond the gun muzzle, both with and without an axial guide field. They include electric probing, space current measurements with Rogowsky loop probes, spectroscopic measurements, particle analysis, diamagnetic measurements from outside the vacuum chamber, high-speed photography, and others. A relatively simple picture emerges in the absence of a guide field, which appears to be consistent with the magnetized plasma expansion model discussed above. In the presence of a guide field the process is much more complicated so that observations and explanations become difficult.

5.1 High-Speed Photography, Muzzle Phenomena

High speed photographs looking directly into the gun muzzle were taken at short time intervals over about 8 μsec from first breakdown (Fig. 24). During the first 2 μsec the appearance of the discharge depends on whether or not there is a bias field, but from then on the presence of bias field makes little difference, and most of the light appears to be localized on the tips of the electrodes. On the center electrode (cathode) the light appears as a bright ring with the tip of the electrode remaining dark for about another μsec. On the outer electrode

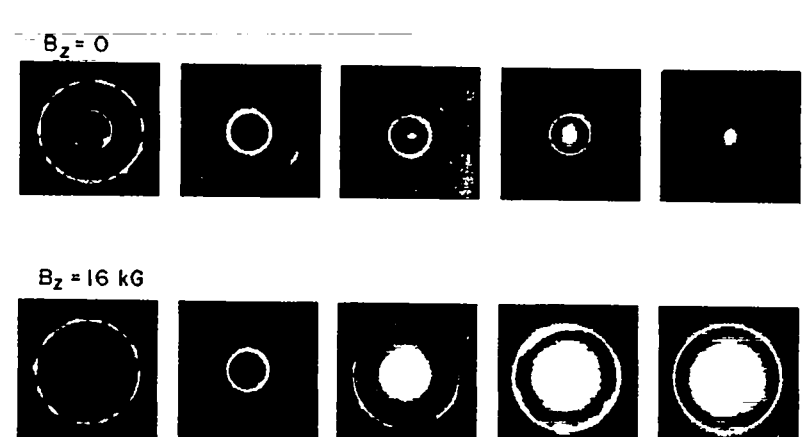

Fig. 24. Image converter camera photographs of gun muzzle. Gun bias field, B_0 = 1.4 kV. The time scale is the same as in Fig. 23. Exposure time 0.05 μsec.

it appears as a number of bright spots, a large number with bias field approximately evenly distributed around the circumference, one to three spots without bias field. Semi-quantitative considerations of ion orbits just inside the muzzle indicate that the outer surface of the cathode is probably heavily bombarded by ions, and this may be responsible for the luminescence. Inspection shows superficial melting of inner electrode near the muzzle. Lovberg has found electron emission unnecessary to explain cathode current under conditions typical of the barrel phase, but his mechanism breaks down at the muzzle, and it may be that electron emission secondary to the ion bombardment is an essential part of the phenomena observed. Recent work by Stratton[3] on the low voltage dc coaxial guns shows that ion orbits are similar to those inferred here and that cathode current is probably due to thermionic emission of electrons.

5.2 Rogowsky Loop Volume Current Probes

The axial current jet from the muzzle of the gun was investigated with Rogowsky loops inserted into the system in appropriately bent glass tubes. The tubes were passed through Teflon compression glands

from the end opposite the gun and could be adjusted in axial position without breaking vacuum. The Teflon glands allowed enough angular adjustment so that the loops could be centered on the axis of the system. Loops of approximately 5, 10, and 18-cm diameter were used. The glass tubing was 8-mm diameter Pyrex. The 10-cm loop was of a size just to slip over the outer gun electrode while the 18-cm loop would just slide inside the glass vacuum wall. Loops and other probes probably disturb the gun plasma at positions downstream from the tip. It is believed, however, that effects on currents and potentials at the tips are small.

In the absence of guide field a jet of negative current grows outward from the center electrode with a speed of about 6×10^7 cm/sec. Within 30-cm of the gun muzzle the current is pinched into a narrow enough stream that all of it passes through a 10-cm diameter circle. The return current appears to pass along the glass wall behind the large diameter Rogowsky loop. Beyond 30 cm the negative space current spreads out so that more passes through the 18 cm than through the 10-cm diameter loop. It is suspected that current and potential phenomena far from the muzzle involve wall effects and would be quite different in a larger system.

With a 16-kG guide field no current is seen with the larger loops. With a 5-cm loop, however, quite a different current system is seen. Within 10-cm of the gun muzzle a negative current jet continues in space, the current along the center electrode. Farther away the current reverses and becomes positive. Since no current is seen with the 10-cm loop, the current through the 5-cm loop must return inside a 10-cm diameter. Presumably the positive current along the axis is due to non-adiabatic behavior of deuterons which have large enough orbits in the field to extend outward from field lines along which electrons from the cathode can accompany them. This produces a sheath of positive space charge and potential, which can then draw in electrons from the anode or from the system wall which is effectively connected to the anode (witness the

return current along the wall). Space current measurements with and without guide field are summarized in Figs. 25 and 26.

5.3 Electric Probes

Plasma potentials were studied by the use of simple passive electric probes inserted through the same seals as the Rogowsky loop probes. The probes were constructed by epoxy cementing copper caps over the ends of glass tubes through which coaxial cable was led. The cable braid was left unconnected at the electrode end, but was grounded to the screen room wall and the center conductor was connected to it through a 100-ohm termination resistor on the probe side of a voltage divider network. The 100-ohm termination was found necessary to reduce noise to a tolerable level. Since probe signals were many kilovolts in amplitude, currents of up to 100 A were drawn from the plasma. The large probe currents apparently distort voltage signals, if they distort them at all, only at very early times when the plasma at the probe tip is tenuous. No difference is seen between signals obtained with 100-ohm and 50-ohm terminators within the reproducibility of the system. Summaries of potential probe observations are given in Figs. 27 and 28 for the measurements with and without guide field.

For the case of no guide field the potentials have first been smoothed by averaging a number of shots at each position, and then have been corrected for inductive voltages due to the changing axial space current. Some of the flux surrounding the current jet also surrounds the probe and should be expected to induce an emf in it which has nothing to do with the potential of the probe tip. It must be emphasized that the plotted potentials, because of the smoothing and correcting which has been necessary, are only approximate. With no guide field the potentials are negative everywhere. This is not too surprising since the anode is grounded and the potentials are measured relative to ground.

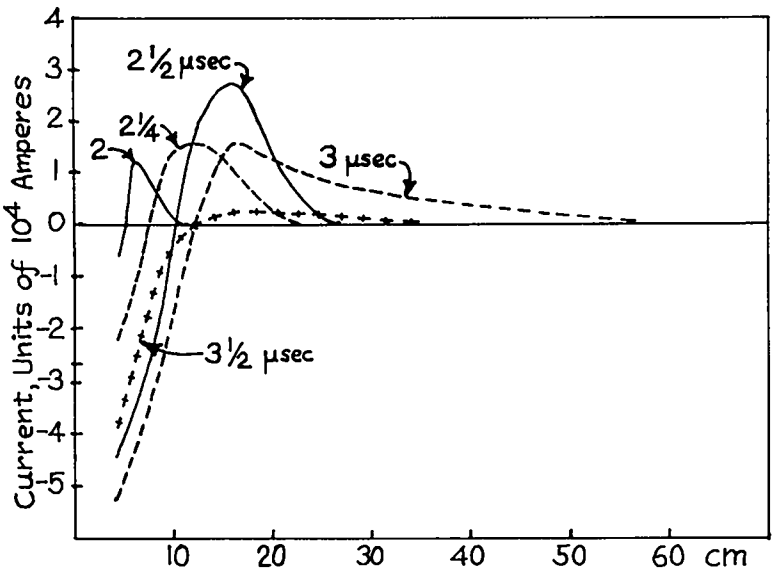

Fig. 25. Plasma current measured with 5-cm diameter Rogowsky loops. Bias field, B_o = 1.4 kG. Guide field, B_z = 16 kG.

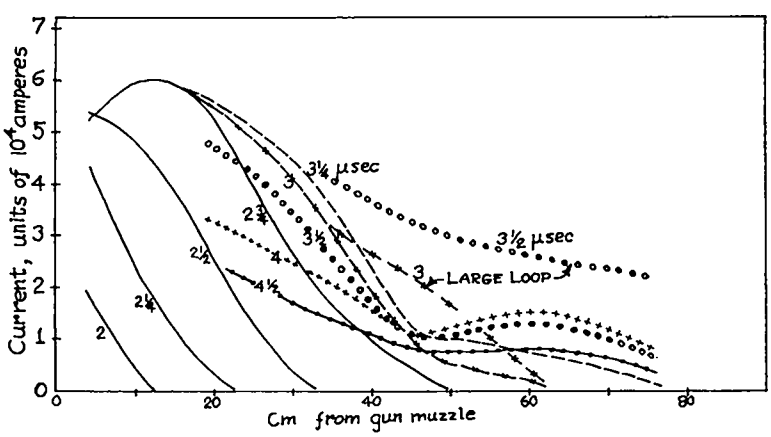

Fig. 26. Plasma current measured with 10-cm and 18-cm diameter Rogowsky loops. Bias field, B_o = 1.4 kG. Guide field, B_z = 0.

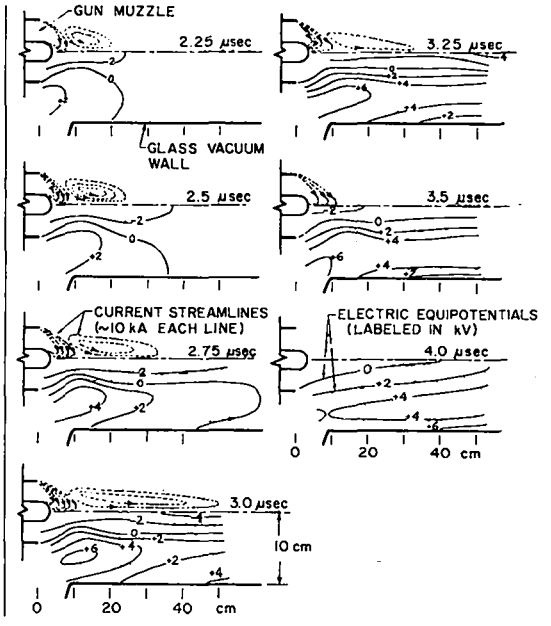

Fig. 27. Potential and current distributions at various times. Bias field, B_0 = 1.4 kG. Guide field, B_z = 16 kG. Note that these represent smoothed data from a large number of shots, and that a considerable amount of imagination has been employed in drawing the current streamlines.

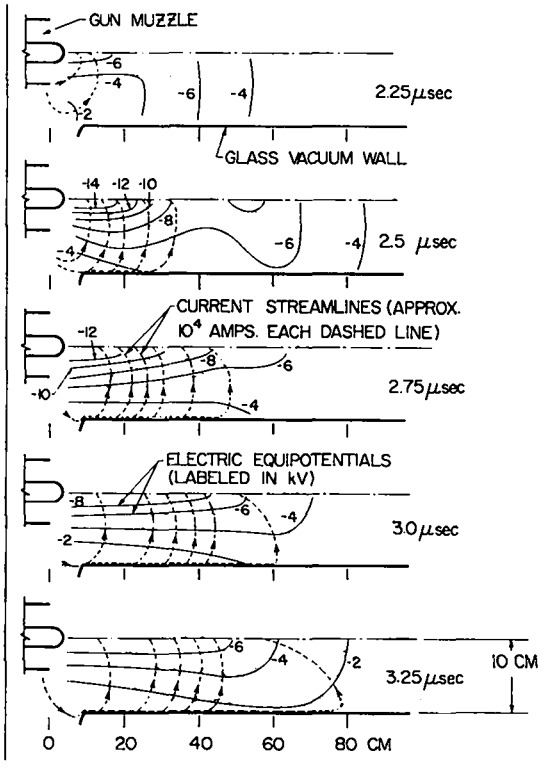

Fig. 28. Potential and current distributions at various times. Bias field, B_0 = 1.4 kG. Guide field, B_z = 0.

With guide field the current system is not so extended or strong as without the field and no corrections have been made for inductive emfs in the probe stems. Considerable smoothing has been necessary, however, for a disturbance at a frequency of approximately 2 Mc which rotates in the $\vec{E} \times \vec{B}$ direction. The disturbance has an amplitude of about 2 kV for probe positions near the gun muzzle, and was observed in three probes when their tips were actually touching the anode 120° apart. The inference is that it is caused by magnetic induction from a rotating current filament.

The frequency of rotation is not unreasonable for the E/B speed inferred from the observed electric fields and applied guide field. The electric potential is negative close to the axis and positive away from the axis. The positive potential off axis presumably is a sheath effect having to do with the large gyro radii of the ions in the guide field, as mentioned above.

The probes indicate high potentials out in front of the current system measured with the Rogowsky loops. The first signal in the absence of guide field moves with a speed of about 2×10^8 cm/sec. With guide field the early signals tend to be noisy and no reliable front velocity has been obtained from the probe data. Another measurement, however, has been made from outside the vacuum vessel by using capacitive pickup electrodes on the surface of the glass. This shows that a positive potential front propagates along the tube with a speed of 4×10^8 cm/sec. The impedance of this measurement is high while the probe results are with low impedance, so there may be no significance to the difference of the front velocities in the two cases.

5.4 Particle Analysis

An ion energy, momentum analyzer using a slit collimator with electrostatic and magnetic deflection was constructed and used on the system with the object of studying impurities. We do not wish to discuss the impurities here beyond the statement that they form a very minor part of the fast plasma with the present system. However, the particle analyzer made it possible to identify deuterons, measure their energies, and determine at what time they arrived at the Faraday cup collector 4.9-m from the gun muzzle. From the known velocities associated with the measured deuteron energies, it was then possible to infer the time at which they left the gun muzzle. The results of these measurements,

made with a 16-kG guide field, are displayed in Fig. 29. It will be observed that the first deuterons appear to leave the muzzle 2 μsec after first breakdown in agreement with the measurements discussed above. The first deuterons are of low energy but the maximum energy observed increases over about the next μsec and then decreases again. The gun muzzle appears to be a source of fast plasma over about the time that a strong current sheath flows between the electrodes. These measurements were made with an instrument capable of detecting only particles on the axis of the system and moving at angles of less than a few degrees from the axis. The deuterons have a broad energy distribution peaking at about 8 keV and extending above 14 keV. It can be seen from the figure that the first deuterons observed by this method to pass the diamagnetic loops are roughly coincident with the beginning of the diamagnetic signals. What appears to be excessive diamagnetic signal at late times is largely due to particles moving with a large fraction of their velocities in the transverse direction where they are outside the analyzer collimation limits. Some particles are stopped and reflected in what amounts to a mirror field produced by plasma diamagnetism in the guide field. The diamagnetism being larger near the gun, the guide field is reduced by a

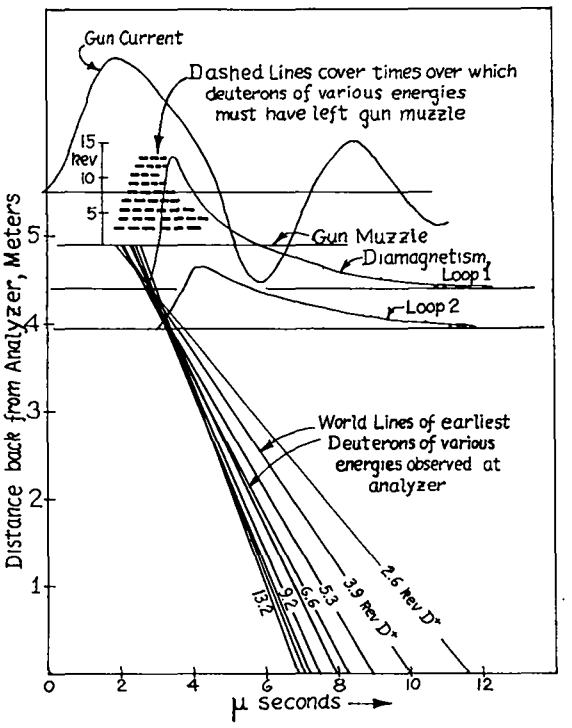

Fig. 29. Axial distance vs time of deuterons of various energies observed by particle analyzer. Diamagnetic signals at two loop positions plotted on same time and distance scale.

larger amount there than it is farther away, and the resulting field rises with distance. Particles so reflected spend a relatively long time at their reflection points and contribute large amounts to late diamagnetism. Peak diamagnetism in the two loop signals plotted corresponds to about 5 and 2.5-J per cm of transverse particle energy, assuming the plasma to be of low β.

5.5 High Speed Photography of Fast Plasma by Secondary Luminescence

High speed photographs were taken of the secondary light produced when the fast plasma is allowed to bombard a glass plate. Under the large energy fluxes involved ($\sim 10^7$ W/cm^2) the surface of the glass evaporates and forms a luminous plasma. The duration of the light following a pulse of fast plasma depends on the presence or absence of a magnetic field, and light production is certainly non-linear with energy delivered, so altogether the method is good only for qualitative information. It will indicate, however, when an energetic plasma first arrives and where. The camera was a fast three-frame image converter unit, the exposures being of 2×10^{-8}-sec duration at 10^{-7}-sec intervals. The amount of light was so large that even at this short exposure it was necessary to stop down the lens to f/70 with a factor 100 neutral filter. A Pyrex disk was used as a target. The side away from the gun was frosted and the disk was viewed from the frosted side so that the gun could not be seen by the camera. Typical results are seen in Fig. 30. First luminescence with a guide field appears on axis, with later light reaching out approximately to the radius of the gun muzzle. The size of the fast plasma column appears to be almost independent of guide field strength except that below 5 kG some of the plasma seems to flute outward producing irregular patterns. Some of the photographs show sickle shaped patterns which are probably associated with the $\vec{E} \times \vec{B}$ rotation discussed above under electric probing. The first plasma to arrive is distinctly faster with large guide field strength than it is when the guide field is small or absent.

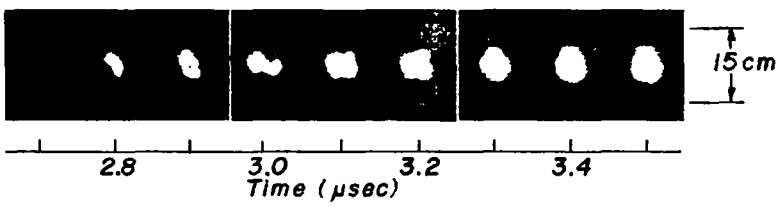

Fig. 30. Image converter camera photographs of secondary luminescence produced by fast plasma bombardment of glass plate 48 cm from gun muzzle. Bias field, B_o = 0. Guide field, B_z = 16 kG. Three gun shots; three 20-nsec exposures per shot at indicated times.

6. Summary and Conclusions

The picture of the fast plasma acceleration mechanism which emerges from the measurements described here is quite different with and without guide field. With no guide field the magnetized plasma expansion model discussed above appears to apply at least qualitatively. Certainly at least the $\vec{j} \times \vec{B}$ forces in the gun muzzle current system must be applied to some reaction force, and there appears to be nothing available for the role except ion inertia. Since current and magnetic field are extended over a large volume in front of the gun muzzle the acceleration must be a gradual one as it would be in the expansion model. According to the expansion model, the streaming velocity of the plasma should everywhere be in the $\vec{E} \times \vec{B}$ direction and its speed should be E/B. Inspection of Fig. 28 shows that the $\vec{E} \times \vec{B}$ direction is substantially forward

with almost a constant value of radial electric field and a transverse magnetic field which decreases with increasing distance from the gun. The expanding plasma, moving in the $\vec{E} \times \vec{B}$ direction should then accelerate gradually parallel to the electric equipotentials. The model breaks down badly in regions where the particles behave non-adiabatically. This is so particularly at the gun muzzle where estimates of particle trajectories show that deuterons starting at rest on the inner surface of the outer electrode pass very close to the surface of the inner electrode so that in fact many of them might be expected to strike it. Bombardment of the inner electrode tip may well be responsible for luminescence observed there during the time of emission of fast plasma and may also account for the large electron currents which probably originate there. The inward trajectories of the deuterons together with the magnetic deflection of their orbits in the forward direction probably account for the apparent small size of the plasma source beyond the tip of the center electrode.

With a 16-kG guide field the magnetized plasma expansion model appears not to apply to the situation at all. The continuation beyond the electrode tips of the currents established along them during the gun barrel phase never reaches out more than about 12 cm. Beyond this the measured current is actually in the opposite direction from the electrode current. This positive current in the neighborhood of the axis might be expected to be present when fast plasma from any laboratory source whatever impinges against the end of an axial guide field. It arises from the relatively large magnetic rigidity of the ions in the end of the guide field which allows them to cross appreciable amounts of field while the electrons cannot do so. Plasma electrons can stream into the field along the axial line, but to the side, where the ions can penetrate because of their large orbits, the electrons cannot come directly from the plasma and a positive space charge results, which can pull electrons in from any available conducting surface along the field lines in question. A mechanism of this sort has been inferred by Ashby[4] from somewhat different

measurements of the currents involved and at much smaller plasma densities. In a situation like this, where the ions and electrons of a plasma actually come from different sources, it would be meaningless even to think of the process as describable by the behavior of a plasma continuum. Instead one must think of the mechanism as involving interdependent but separate non-adiabatic behavior of electrons and ions. Under such conditions there is no difficulty in understanding the thorough mixing of fast plasma and field which first appeared rather mysterious when the plasma was considered from a hydromagnetic viewpoint.

When the gun is fired into the guide field nearly all of the fast plasma acceleration occurs at the gun muzzle or very close to it. This follows from the direct observation that the entire current from anode to cathode closes close to the muzzle. The $\vec{j} \times \vec{B}$ forces which must be responsible for the acceleration occur only in this region. In the positive current whorl inside the guide field there is probably a further acceleration of a part of the plasma to higher speeds at the expense of some of the ions which get slowed down or turned back. The basis for this statement is not very solid and in any case the effect is probably not a large one. The acceleration process with the guide field is obviously more complicated than without it, and many details are not yet understood.

7. Acknowledgments

The authors are most grateful for the assistance of R. W. Kewish, Jr., in the accumulation and reduction of data, to B. E. Burkheimer for technical assistance, and to E. L. Kemp and A. S. Rawcliffe for engineering support. Many other members of the laboratory have helped by scientific discussion. In particular, thanks are due to D. A. Baker, J. E. Hammel, J. McLeod and J. L. Tuck.

---

[1]Marshall, J., Phys. Fluids 3, 134 (1960).

[2]Marshall, J. and Stratton, T.F., Nuclear Fusion Suppl. Pt.2, 663 (1962).

[3]Stratton, T.F., Private Communication.

[4]Ashby, D.E.T.F., Bull. Am. Phys. Soc. Ser 3, 9, 331 (1964).

TRANSVERSE INJECTION

(J.E. Hammel)

Electric Field Measurements

As mentioned in the preceding Semiannual Report (LA-3320-MS, p. 71), a more complete study of the electric fields produced by a gun plasma stream as it crosses a magnetic field was proposed as a means of understanding the entrance of the stream into the transverse B-field. The 30-probe readout system was not successful as tried because of voltage breakdown in the external circuit. However, electric field measurements with eight probe pairs show some of the more complicated features of the polarized stream. The electric fields are measured by multiple probes outside the magnetic mirror with the probes placed at various positions along the stream direction. Figure 31 is a plot of the peak electric field as a function of B for probes 12-cm and 7-cm ahead of the axis of the B-field and the same distances behind the axis. Since the transverse field is essentially at its vacuum value during the passage of the fast plasma, E/B gives the velocity of the stream.

Velocity Dispersion in the Magnetic Mirror Field

For magnetic field values below 3.5 kG it is observed that the peak velocity of the stream becomes progressively larger as the stream proceeds through the field. An effect which might produce a velocity change such as the one observed arises from the variation of the magnetic field across the plasma in the field direction. The change in E/B can be derived by considering a tube of flux with a width Δr_1, at a radius r_1 from the field axis at the midplane and a width Δr_2 at a radius r_2 off

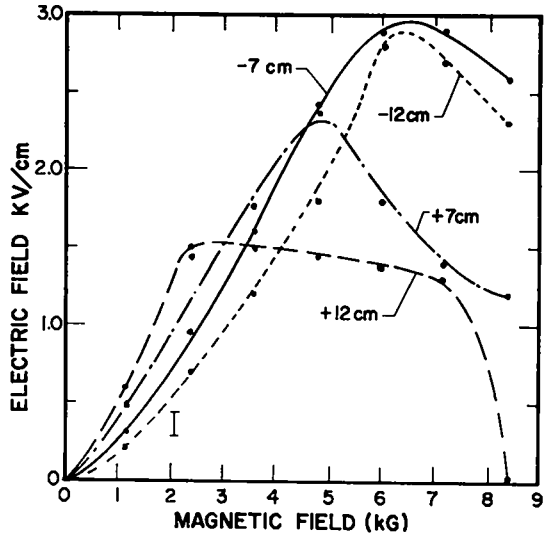

Fig. 31. Peak electric field as function of magnetic field for probes 7 cm and 12 cm ahead of and behind magnetic axis.

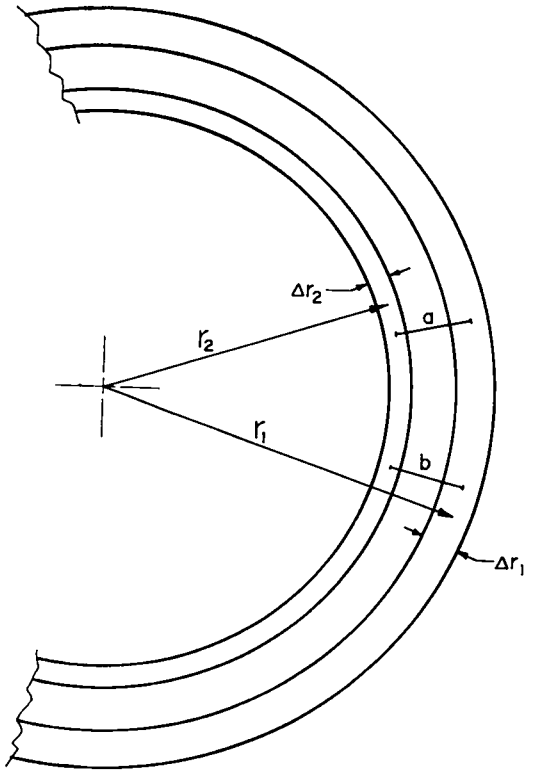

Fig. 32. Portion of tube of flux.

the midplane toward the magnetic mirror (see Fig. 32). The field strengths at the two positions are related by

$$r_1 \Delta r_1 B(r_1) = r_2 \Delta r_2 B(r_2). \tag{1}$$

Two nearby field lines (a and b, Fig. 32) within the tube of flux will have a separation at these two positions proportional to the radii, r_1 and r_2, and since magnetic field lines are lines of equal electric potential, the electric fields will be related by

$$E(r_1) r_2 = E(r_2) r_1. \tag{2}$$

Using Eqs. (1), (2), and E/B = v, the plasma velocities are given by

$$v(r_1) = \frac{\Delta r_1}{\Delta r_2} \; v(r_2).$$

The injected plasma will adjust itself to these velocities through current flow with the j x B forces accelerating the plasma at the midplane and decelerating the plasma well off the midplane.

In the geometry of the experiment the velocity of the plasma at the midplane could be as much as 1.4 times the input velocity. The velocity increase observed up to 3 kG in Fig. 31 could be explained by the plasma of higher velocity at the midplane outrunning the remainder of the plasma and giving the higher electric fields observed downstream.

Stream Stopping

At high fields quite a different effect is found since the plasma velocity is observed to decrease as it moves through the field. In previous experiments, it was found that depolarization currents along the glass insulators at the input played an important role in inhibiting the penetration of the plasma into high magnetic fields. The present results show, however, an attrition of the plasma flow well after it has passed the insulator region.

It might be expected that the most likely process for the stopping of plasma drift by a large transverse field would be through the adiabatic increase in perpendicular energy as it moves into the high field region. However, this process cannot be responsible for the result found here, since the plasma moves through the position of peak field at the axis and passes the downstream probe position with progressively lower velocity (the rear probes are placed at the same distance beyond the field axis as the front probes are forward of the axis). The explanation for the slowing and stopping of the stream at very high magnetic fields is not known but it is felt that it must be associated with line-tying by plasma or by a surface outside the magnetic mirror.

EQUIPMENT DEVELOPMENT AND TESTING

Dielectric Switches (I. Henins, R. Kewish, Jr., and J. Marshall)

Introduction

As the energy storage systems in use become larger, the reliability of components becomes more important. Solid dielectric switches, in which the insulation is mechanically destroyed during switching, promise to be more reliable than spark gaps or ignitrons as far as prefiring is concerned. Considerable development of this type of switch has been done at the Culham Laboratory in England where a bridge wire is exploded to rupture the insulation and the switch contact is made through the subsequent arc. Another slower type used for crowbar applications uses an electromechanically-driven rivet to break the insulation and then make a permanent metal-to-metal contact between the conductors.

High-Explosive Driven Switches

It is reasonable that a high-explosive charge could also be used to rupture the insulation to produce the arc contact, or possibly to drive one of the conductors through the insulation to make a direct contact with the other conductor. Some high-explosive driven, high-current switches of the arc type are in existence at LASL, but generally they are too expensive for use in most Sherwood applications. The first impulse has been to develop an inexpensive explosive driven switch that would be

suitable for Sherwood switching requirements in having a suitably low inductance and resistance and small jitter. The development of the explosive driven switch is being pursued in cooperation with GMX Division at LASL.

Exploding-Foil Driven Switches

High explosives are dangerous even in small amounts and necessitate rigid safety and handling procedures which make their use inconvenient. Since Sherwood personnel are already prepared to cope with electrical explosions, it is certainly more attractive to use exploding foils or wires to drive one conductor of the switch through the insulation to produce contact with the other terminal. Initial efforts in this direction have been quite successful.

The device described below has been used both as a closing switch and as a crowbar switch. As a closing switch it has carried, without arcing, a current of approximately 1.2 MA. The initial voltage across the switch was about 7 kV and current rise time about 30 μsec. As a crowbar it has closed with no voltage across the switch and carried about 100 kA. The switch closes about 15 μsec after the application of power to the exploding foil and the jitter appears to be about 1 μsec. The time delay and jitter are a function of the thickness of insulation to be broken, the initial geometry and mass of the exploding foil, and the energy input to the foil. At the present, further tests are necessary to determine the reliability and performance characteristics of the switch.

The present switch is shown in Fig. 33 and consists of a 2.5-in. long, $\frac{1}{4}$-in. wide, 0.002-in. thick Cu foil insulated by 0.030 in. of polyethylene clamped against the back of a $\frac{1}{8}$-in. thick annealed soft Al plate. The foil is exploded by a capacitor bank charged to 15 kV and

storing about 5 kJ of energy. The explosion pressure of the foil forces the Al plate into a die which is also one terminal of the switch. In the process the 0.030-in. polyethylene insulation between the plate and die is sheared and contact made. The die has a longitudinal groove milled in it the same width as the exploding foil and 3/32-in. deep. In addition, four 1/4-in. x 3/8-in. oblong holes in the bottom of the groove provide pressure relief and additional space for the Al to jam into. The connection of the Al plate to the other terminal is so arranged that the magnetic field forces after switch closing tend to hold the contact closed.

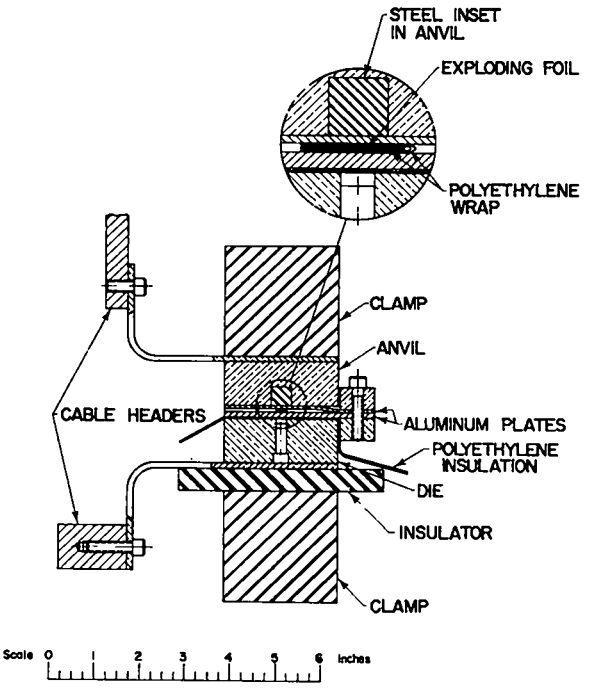

Fig. 33. Exploding-foil driven switch.

Current Interruptor for Magnetic Energy Storage (I. Henins, R. Kewish, Jr., and J. Marshall)

Considerable effort has been expended during this period on the development of a practical current interrupting switch for inductive energy storage. This type of storage has apparent advantages when very large amounts of energy are to be transferred, and the unfavorable volume and expense required for capacitive energy storage become important. Present capacitive storage systems begin to suffer seriously from reliability difficulties at 10 MJ and over. The difficulty is that considerable development is required in the switching for inductive storage and that somewhat special facilities are required for testing during the development.

A discussion of inductive energy storage has been given in previous reports (LA-3202-MS and LA-3320-MS). Following the train of thought expressed previously, the requirement assumed is to open a switch carrying of the order of 10^5 A with a capacitor bank across the switch terminals so that the voltage at interruption time is small. After break, the current initially transfers into the capacitor bank to produce a rising voltage across the switch. Energy transfers to the load in parallel with the switch and the capacitor at the same time, and not all of the initial energy must be stored by the capacitor. A practical arrangement, with the load inductance half that of the storage inductor, requires 3/8 of the energy finally transferred to the load to be stored temporarily in the transfer capacitor.

A practical energy storage system would involve the slow buildup of energy in the storage system over a period of about a minute. Thus the switches have to be able to carry steady currents. Obviously the interruptor can be paralleled with a slower acting high-current switch so that its requirements in this direction are somewhat reduced. To provide the large currents required of a practical interruptor, an ignitron switched capacitor bank has been used. The test circuit initially was as shown in Fig. 34. Although the energy stored by the capacitor bank is very small compared to the energy considered in the inductive storage system, practical currents and rates of voltage rise can be achieved by varying the inductance and the size of the passive capacitor.

The switch was designed to have high opening speed combined with a high-pressure N_2 gas blast. It employs compressed N_2 to drive a sliding contact at high speed out from between a pair of conducting rails. The gas is contained initially in a cylindrical pressure vessel with a Mylar rupture diaphragm at one end. The two rail contacts and a pair of phenolic slabs form a rectangular gun barrel 1½ in. square along which the contactor is driven to high speed by the N_2. The contactor is simply

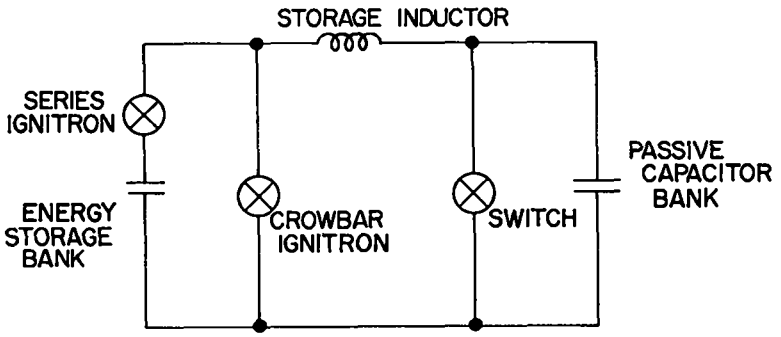

Fig. 34. Test circuit for interruptor.

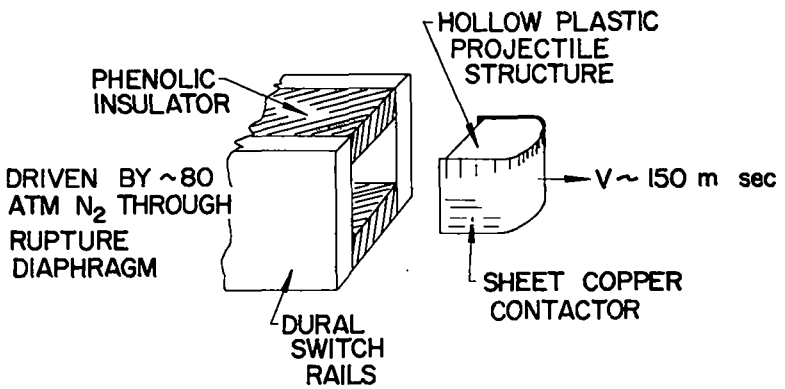

Fig. 35. Current break portion of switch.

a strip of Cu folded over the bottom of an open plastic box projectile structure. The plastic (epoxy and glass fiber) projectile is recoverable, while the Cu contact strip is replaced for each shot. At the end of the gun barrel the projectile is observed to emerge with a speed of 150 to 200 m/sec depending on N_2 pressure. The high-pressure gas blows past the arc region between contactor and switch rail, and presumably helps in extinguishing the current. A sketch of the current break part of the switch is given in Fig. 35. The projectile is decelerated in a catcher box filled with wadded cheesecloth. The projectile moves with a speed comparable with that of a pistol bullet, and so must be treated with care. The gun barrel is approximately 35-cm long and the projectile requires about 2 msec to reach the muzzle after the diaphragm breaks. Sufficiently accurate timing of current break relative to triggering of the energy storage capacitor bank is achieved by sensing the rupture of the diaphragm. This is done with a small pressure sensitive switch. Variations of projectile velocity are not too serious because of the crowbarring of the inductor current.

No trouble was found in opening the switch at less than 2×10^4 A. A successful switch opening produces very little arcing at current break, the arc extending for no more than about 1 cm and the current being opened in ~ 50 μsec. Current and voltage behavior in the test circuit are shown in Fig. 36 for a shot in which 21 kA current was interrupted with an initial rate of voltage rise of 12.5 kV/msec. Currents greater than 30 kA have been successfully broken but only at somewhat reduced voltage rise rates. A current of $2\text{-}3 \times 10^4$ A is quite large, but to reach energy levels of prime interest it should be possible to break currents about ten times larger. Conceivably the switch dimensions could be increased to raise the current rating, but this would probably produce a very cumbersome device. Instead, work has been directed toward modifications of the circuit making it unnecessary to break so large a current.

In seeking a means for extending the current range of the switch, the use of magnetic fields was considered. A static field in the region where interruption takes place can apply a $\vec{J} \times \vec{B}$ force to the arc so as to aid the N_2 blast in blowing it out. In addition, the moving contactor and arc produce a $\vec{v} \times \vec{B}$ electric field which opposes the inductive emf maintaining the arc. For an application such as this, a pulsed magnetic field is more suitable than a steady one and it would produce inductive electric fields which could be arranged by suitable timing to oppose the arc current and perhaps extinguish it. The most direct way of driving the magnetic field to provide this back emf would be to introduce the current into the switch circuit itself. This chain of reasoning has led to the circuit of Fig. 37.

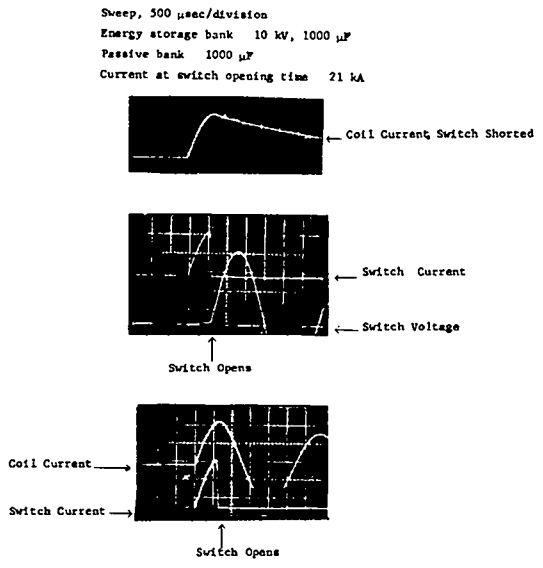

Fig. 36. Current and voltage vs time in current interruptor test.

An artificial delay line is connected across the switch through an ignitron which is triggered just prior to current interruption time by a mechanical contact with the projectile. The delay line is dc-charged to a voltage adjusted so that the current delivered by the line to the switch is as nearly as possible equal and opposite to the current already flowing through the switch from the storage inductor. If the switch current is thus reduced to less than 20 kA, the switch should open, and if the reverse current is maintained for a long enough time

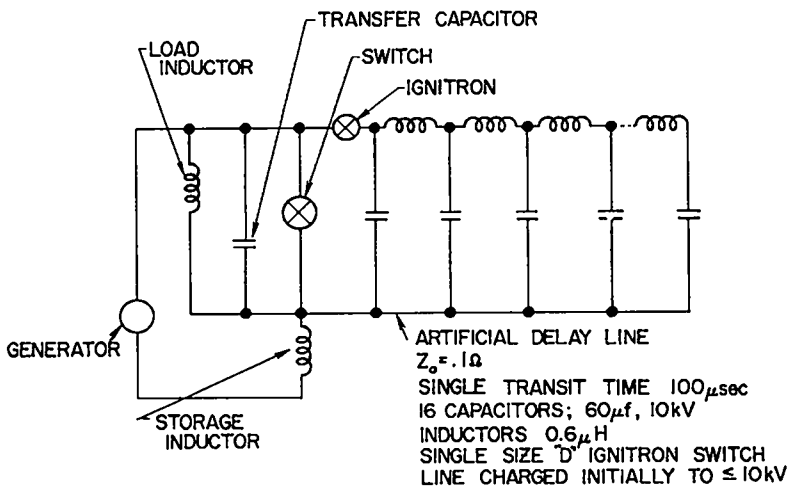

Fig. 37. Energy storage switch with artificial delay line.

for the switch to be well open, the arc should not restrike. This circuit, with the substitution of the ignitron switched and crowbarred capacitor bank of Fig. 34, has been tested and found to allow the N_2 driving switch to open 40 kA. The bank is too small to provide a good simulation of the generator driven case, and a larger bank is being prepared.

There seems to be no obvious reason why a system of this sort should not be successful. It will be necessary to be sure, however, before proceeding to the engineering design of a large, expensive machine. Work directed toward this end will be done as the manpower becomes available.

Capacitor Development (G. Boicourt and E. Kemp)

Scyllac will require a 2-μF, 60-kV capacitor for the main bank. A program has been initiated to develop and test such a capacitor. Three capacitor manufacturers have been asked to build test units. One has

delivered two units and these have been tested in the new 75-kV test bay. They had lives of two and five shots, respectively, and there is evidence that they would not have operated even at 50 kV. Since this design is essentially the same as the well-tested 2-μF, 50-kV unit, it appears that the trouble lies in the assembly and not in the design. A 2-μF, 50-kV unit of the same manufacture was subsequently tested and it had a life of over 1800 shots.

Testing has been also carried out on a variety of other capacitors. These include 5-μF, 25-kV high-density units; 2-μF, 50-kV units; on-side testing of 60-μF, 10-kV units; 180-μF, 10-kV high-density units; and 14.2-μF, 20-kV low-inductance units.

Low-Inductance, High-Voltage Cable (G. Boicourt and E. Kemp)

The poor performance of 17/14 and 17/14-G cables in Scylla IV has made it imperative that a better cable be developed for Scyllac. The problems have been discussed with several cable manufacturers and a number of possible solutions suggested. These include better quality control, high-voltage screens of several designs, and laminated dielectric cores. Steps have been taken to purchase modified designs which the particular manufacturer seems best equipped to produce. A testing plan to evaluate these cables has been established and the first phase has been completed.

In the phase I test, standard 17/14 cables were connected as shown in Fig. 38; the equivalent circuit is given in Fig. 39. Computer runs show that the test cable is subject to 78 kV at the C_c end and to 65 kV at the spark gap. A plot of n/n_o vs log S for 46 cables which were tested is given in Fig. 40; n_o is the total number of cables tested, and n is the number of cables remaining after S shots. The straight line is reasonably well fitted by the equation

$$n/n_o = 1.6 - 0.4 \ln S.$$

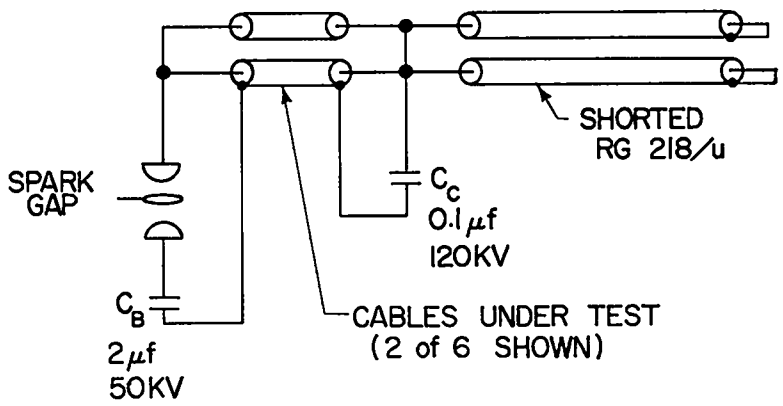

Fig. 38. Connections for 17/14 cable tests.

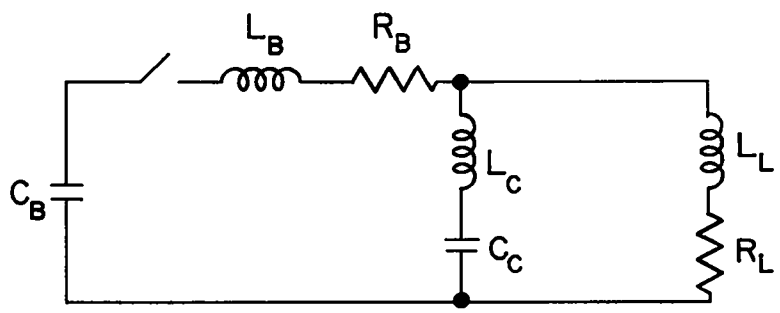

Fig. 39. Equivalent circuit for cable tests.

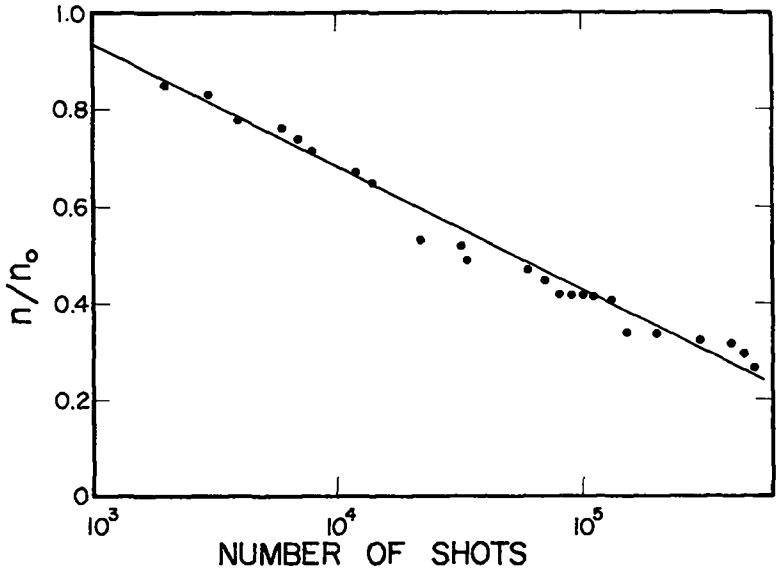

Fig. 40. Results of cable tests.

In the phase II test, which has been initiated, six cables in parallel attached at the doubling capacitor C_c are added and left open-ended to produce voltage-doubling at the open end. This setup also simulates actual cable use since it is the same hookup which appears when a crowbar is attached to an experiment by cables.

Current Connectors (G. Boicourt)

Two types of current connectors for Scyllac have been tested. A sample of one, a single cable, plug-in connector, was tested for over 30,000 pulses, carrying more than 10 kA per pulse. The second was a cartridge current connector which must carry the current from nine cables (see Fig. 12). A sample was tested for 3000 pulses carrying 90 kA per pulse.

NEW MATHEMATICAL PHYSICS GROUP

(W. B. Riesenfeld)

Organization

A mathematical physics group, designated P-18, was formed on September 1, 1965 in order to give a more formal organizational base for mathematical-theoretical Sherwood activities. The purpose of the new group is to provide theoretical support for the experimental Sherwood effort, as well as to investigate problems which may be of special interest to the members of the group. These are D. A. Baker, R. Lewis, R. Morse, W. Riesenfeld (Group Leader), E. Stovall, E. Woollett (Postdoctoral Fellow), and Judith Wagner (Data Analyst). Group Secretary is Gladys Alexander, and T. Oliphant (T-9) is collaborating with the group on some computer-oriented problems.

Summary of Activities

Among the problems attracting immediate attention are the questions of designing closed magnetic field configurations possessing desirable equilibrium and stability features, extensions of containment theory to higher β regions, and the development of stability criteria for more realistic plasma models than the hydromagnetic and single-particle pictures. These problems are directly related to the design of the toroidal Scyllac device as well as to the preliminary sector experiments, and therefore both numerical and analytical studies of $\int d\ell/B$ stable, closed magnetic field geometries (by D. Baker and W. Riesenfeld) are in progress. The susceptibility of such systems to localized hydromagnetic

interchange (ballooning) is being considered, a figure of merit being the critical β_c for which the instability may occur. The value of β_c can be directly estimated on the basis of magnetohydrodynamics using certain geometrical parameters of the lines of force. A more realistic value of β_c may be expected from a theory which explicitly includes finite ion gyration radius effects, and this direction of investigation will be pursued. Resistive ballooning for $\beta < \beta_c$ does not appear to give damaging growth rates for the contemplated electron temperatures, even when plasma flow along magnetic field lines is neglected.

The problem of high-β equilibrium of free plasma-magnetic field boundaries is also being examined numerically, with T. Oliphant adapting an iteration procedure originally devised by D. Beard for the study of the structure of the interaction region of solar plasma with the earth's magnetosphere. This adaptation and generalization of an astrophysical theory to laboratory-scale plasmas is of unusual interest.

Another numerical field calculation program (R. Lewis), applicable to the nonzero absolute field minimum configuration of the caulked, stuffed cusp, has progressed to provide additional field details and is justifying the vacuum field design.

R. Morse is studying the end losses from a linear θ-pinch with mirror field, on the basis of a self-consistent kinetic theory method, with specialization to both long and short pinches. A generalization to the case of a toroidally curved θ-pinch is desired, but greatly complicated by the loss of the P_θ canonical angular momentum as a constant of motion. R. Lewis and R. Morse are investigating the nature of the adiabatic invariants in toroidal geometries.

Topics in kinetic theory are being studied by E. Woollett, with attention to the small-angle, laser light scattering experiment on Scylla III. This experiment is expected to produce information on the ion velocity distribution; if the latter is not thermal, then a more detailed theory is required for interpretation of the results.

INVESTIGATION OF $d\ell/B$ STABLE CLOSED SYSTEMS

(D. A. Baker)

Investigations are being made into the possibility of producing a practical, closed, $\int d\ell/B$ stable magnetic bottle for use with a toroidal Scylla device. The work is concerned with the possible design of a relatively simple system of the alternating quadrupole type. Numerical calculations of the fields produced by arrangements of straight conductors have been performed on the IBM 7030 computer using a modified version of the MAGCO code of W. Perkins and J. Brown (LRL). A set of current carrying conductors arranged as shown in Fig. 41 has been found capable of producing a maximum of $W \equiv \int d\ell/B$ on the z-axis. The system consists of a uniform field in the z-direction and a system of alternating quadrupole sections of equal length. Some cross feed currents are directed so that the field is strengthened in the "bad" curvature region and weakened in the "good" curvature ones, thus weighting W to produce a maximum on the axis. A sample set of field lines in the y-z plane is shown in Fig. 42. The calculations neglect the feeds which must supply current to the system at each of the vertices, although it is known that these feeds have adverse effects on stability. A study of the problem including these feeds is in progress.

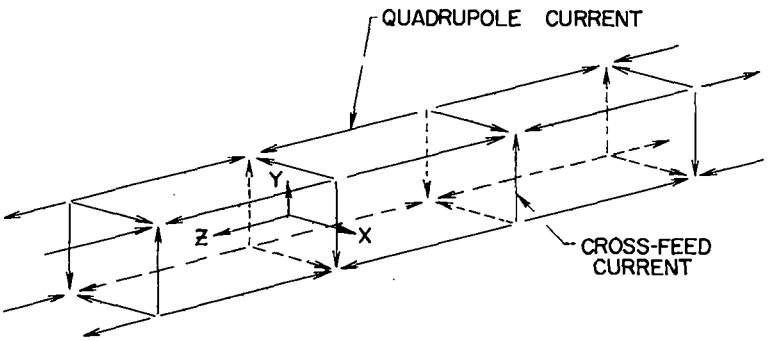

Fig. 41. An arrangement of currents whose fields, when added to a uniform field in the z-direction, produce a maximum in $\int d\ell/B$ along the z-axis.

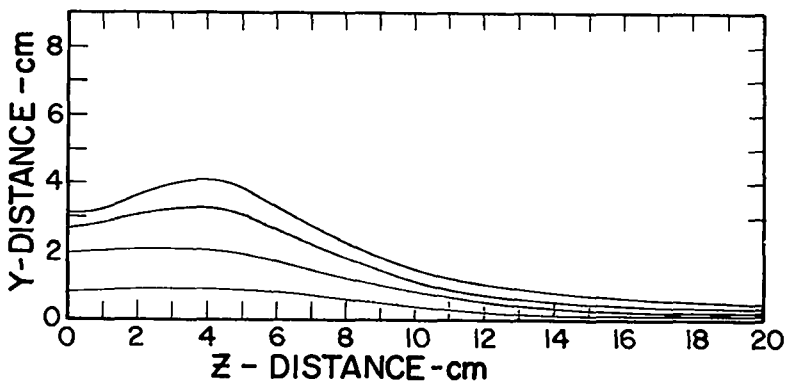

Fig. 42. Set of field lines lying in the y-z plane produced by the current configuration and coordinate system of Fig. 41. The field plot is symmetric about the z-axis. A reflection about the y-axis yields the plot for one period of the field. The plot extends over a distance of one quadrupole section and corresponds to quadrupole currents passing through the corners of a 10-cm square. All current magnitudes are equal. The ratio of quadrupole current to the added uniform B_z is 20 A/G.

PLASMA BOUNDARY CALCULATIONS

(T. A. Oliphant)

The problem is being studied of finding the equilibrium configuration of a $\beta = 1$ plasma in a model calculation for the projected toroid machine. The plasma is assumed to be a perfectly conducting fluid, and the situation then reduces to a magnetostatic problem with a free boundary surface. The problem is treated by the iterative method proposed by Beard et al., in 1964. As a first step, calculations are being made of the cusped equilibrium surface of a plasma confined by a magnetic quardupole field. This phase of the work is well advanced.

COMPUTATION OF ELECTRIC AND MAGNETIC FIELDS

(K. R. Crandall and H. R. Lewis)

The method for computing electrostatic and rapidly pulsed magnetic fields, discussed in the previous Semiannual Report (LA-3320-MS, p. 6) in connection with caulked cusp geometries, has been extended and refined. The problems that can be treated have either axial or translational symmetry. In the magnetic case, currents are assumed to be all azimuthal when there is axial symmetry, and all parallel to the symmetry direction when there is translational symmetry. Loop and line sources (i.e., loop currents or charges and line currents or charges) of prescribed strengths are allowed. The shapes of boundaries may be chosen arbitrarily. In the electrostatic case, the electrostatic potential is specified on boundaries and the effect of surface charges is approximated by loop or line charges together with charges at infinity. In the magnetic case it is assumed that the magnetic field is tangent to boundaries, and the field is determined by specifying constant values of rA_θ or A_z on the bounadries. The effect of surface currents is approximated by loop or line currents along with currents at infinity. The locations of loop and line sources are chosen on the basis of intuition and experience, and the strengths of these sources and of the sources at infinity are determined by a weighted least squares satisfaction of the boundary conditions. The result is an exact and analytic solution of Maxwell's equations which approximates the boundary conditions. The suitability of the approximation is assessed by graphing equipotential surfaces or magnetic flux surfaces of the solution and comparing them with the boundaries which were to be fitted.

Two FORTRAN-IV computer codes for applying this method, details of which will be published shortly (e.g., LA-3416), are available for use on the IBM-7030 STRETCH computer. With one of the codes, solutions of the equations are determined, and equipotential surfaces and magnetic flux surfaces can be graphed. With the other code, a solution can be used for detailed graphing of equipotential surfaces or flux surfaces, and certain integrals can be evaluated, namely, $\int \vec{B}.\vec{d\ell}$ and $\int d\ell/B$ on magnetic field lines, and $\int \vec{E}.\vec{dA}$ on equipotential surfaces. The graphs and integrals can be obtained for a superposition of the field with as many as four other fields which can be chosen arbitrarily. The method has been successfully applied to experimental situations of interest at LASL.

MAGNETIC MOMENT SERIES

(H. R. Lewis)

It has been possible to formulate Kruskal's method for calculating higher order terms in the magnetic moment series in a way that the various operations, including integrations over phase angle, can be reduced to simple (although involved) algebraic operations. A FORMAC computer program (which performs literal algebra) is being constructed for carrying out the procedure.

THERMONUCLEAR REACTOR BLANKETS

(G. I. Bell)

In thermonuclear reactors which burn D-T, economic operation would require that more T be produced than is consumed in the D-T reactions. The reacting plasma might then be surrounded with a thick blanket in which incident 14-MeV neutrons are used to produce T. A series of 25-group DSN calculations has been made to examine T regeneration in various blankets.[1] For thick (> 1 m) blankets of natural Li, it was found that ≤ 1.9 T's are produced per 14-MeV incident neutron by the $Li^7(n,n'T)\alpha$ and $Li^6(n,T)\alpha$ reactions. However, it is possible both to decrease the blanket thickness and to achieve better regeneration ($T \leq 2.9$) by making the blanket mostly of Be with only enough Li present to capture the slow neutrons. The $Be^9(n,2n)2\alpha$ reaction is responsible for this improvement.

Some more practical blanket designs were considered with shells of Cu or Mo between neutron source and blanket and with blankets composed of various combinations Be, Be_2C, Li, and molten fluorides of Be and Li. In all cases considered, if sufficient Be is used, good T regeneration is achieved, while for some designs even Be is unnecessary. As an example, a 60-cm thick blanket of 50 v/o Be and 50 v/o Li having 3.3 cm of Mo between source and blanket gave T = 1.79.

---

[1] G. I. Bell, LA-3385-MS (1965).

PUBLICATIONS

Mather, "Formation of a High-Density Deuterium Plasma Focus," Phys. Fluids, 8, 366 (1965).

Baker and Hammel, "Experimental Studies of the Penetration of a Plasma Stream into a Transverse Magnetic Field," ibid., 8, 713 (1965).

Little, Quinn and Sawyer, "Plasma End Losses and Heating in the 'Low-Pressure' Regime of a Theta Pinch," ibid., 8, 1168 (1965).

Kemp and Dike, "Design of a Low-Inductance Capacitor and Switch Assembly," Rev. Sci. Instr., 35, 516 (1964).

Baker, Hammel and Jahoda, "Extension of Plasma Interferometry Technique with a He-Ne Laser," ibid., 36, 395 (1965).

Dike and Kemp, "Quick Closing Light Shutter," ibid., 36, 1256 (1965).

Thomas, Peacock and Sawyer, "Time-Resolved Spectroscopy in the Far-Vacuum Ultraviolet (100-500 Angstroms)," Soc. Appl. Spectry. Conf., Denver, Aug 1965. Abstracts, p. 47, 1965.

Dreicer, "Technical Proposal for a Research Tool Involving Thermally Ionized Plasma: a Meshed Microwave Resonator Probe," 12 p. LGI-65/5 (1965).

Suydam, "Finite Larmor Orbit Stabilization," LA-3260-MS.

Powers and Ribe, "Computer Program for Solution of the Energy Balance and Heat Transfer of a Pulsed Thermonuclear Reactor," LA-3347-MS.

Bell, "Neutron Blanket Calculations for Thermonuclear Reactors," LA-3385-MS.